Large Deviations and Slow Dynamics in Classical and Quantum Systems

Piper Fowler-Wright

06 May 2020

Contents

1 Introduction

Many important physical processes, including the formation of amorphous solids known as glasses, are dominated by slow dynamics. Without dynamical information, standard approaches from statistical mechanics cannot provide a description of these processes. Such information is incorporated through the analysis of dynamical observables, readily performed within the framework of large deviation theory. The purpose of this essay is to investigate how *local kinetic constraints can give rise to slow and generally complex dynamics.* A summary of its content follows.

In Section 2, aspects of the theory of large deviations are introduced, including the basic mathematical ideas and notations used throughout the essay. This is accompanied by an overview of the *glass transition.* Describing the slowdown and dynamical arrest observed in many soft materials, the origin of this transition remains a major open problem in condensed matter physics and is prime motivation for our studies.

The glass transition problem prompts us to introduce *kinetically constrained models* (KCMs), simple lattice models of glass formers and the subject of Section 3. Two prominent examples of KCM are considered in detail: the Fredrickson-Andersen model and the East model. The time evolution of these models is that of continuous time Markov chains. Accordingly, we develop tools to study the dynamics and large deviations of this class of systems, building on the theory set out in Section 2. This section culminates with the proof of the existence of *dynamical phase transitions* in the models. of *dynamical phase transitions* in the models. The nature of this result and its importance for the glass transition problem is discussed.

With Section 4 there is a shift in focus as we look to explore the consequences of the same mechanisms of constrained dynamics in *quantum* systems. A quantum East model provides a natural link with the previous part and an example of slow dynamics in a quantum setting. We discuss the relevance of the model to the phenomenon of *many-body localisation* in closed quantum systems.

To conclude, current research directions in both classical and quantum domains that the reader may be interested to pursue are presented in Section 5.

When writing this essay effort was made to include references to review material and other relevant work wherever possible. As such, the final reference list is lengthy and it is worth bringing to attention the main source material for each section. Our coverage of large deviation theory is based on H. Touchette's review of the subject [1], complimented by R. Jack's discussion of time-averaged quantities [2]. The theoretical perspective of J. Garrahan [3] was used in conjunction with R. Zallen's textbook [4] on amorphous solids to provide a complete physical picture of the glass transition. Section 3 follows the 2009 paper [5] by J. Garrahan et al. of which the existence of dynamical phase transitions in KCMs was the principal result. Finally, in Section 4 the 2015 article [6] by M. van Horssen et al. is the focus as the original work on the quantum East model.

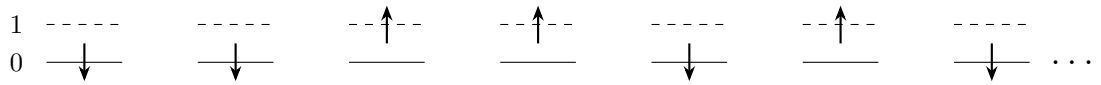

Figure 2.1: Line of random spins. Each spin is excited ($\sigma_i = 1$) or relaxed ($\sigma_i = 0$) with equal probability. In Section 3, dynamical rules are added to this system to obtain the one-dimensional Fredrickson-Andersen and East models.

2 General Theory and Motivation

2.1 Large Deviation Theory

Large deviation theory handles the exponential decay of probabilities of large fluctuations or deviations in stochastic processes. The mathematics were predominately developed by the pairs Donsker and Varadhan [7] and Freidlin and Wentzell [8] in the 1970s, but quickly found a place in physics with, in particular, Ellis' 1985 book [9] establishing a clear structure for its use in the formulation of problems in statistical mechanics.

The aim of this section is to introduce the key tenets of the theory and those aspects relevant to our study of slow dynamics. The treatment is a heuristic one, with emphasis on physical intuition rather than mathematical rigour. A complete presentation of the theory may be found in the book by Hollander [10] or Deuschel and Stroock [11]. Ellis himself provides a thorough overview [12] on its use in statistical mechanics for which the review by Touchette [1] is also an excellent reference.

2.1.1 The Large Deviation Principle

The central concept in large deviation theory is the *large deviation principle.* To appreciate it, consider the line of independent spins shown in Figure 2.1 where each spin takes the value $\sigma_i = 1$ (excited) or $\sigma_i = 0$ (relaxed) with equal likelihood. A quantity of interest is the fraction of excited spins or excitation density

$$S_N = \frac{1}{N} \sum_{i=1}^{N} \sigma_i \tag{2.1}$$

Since the spins are uncorrelated and free from bias, the probability that S_N takes the value $r = k/N$ $(k = 0, 1 \ldots, N)$ follows the binomial distribution:

$$P\left(S_N = r\right) = \frac{1}{2^N} \frac{N!}{(rN)!\,[(1-r)N]!} \tag{2.2}$$

One might look to determine the statistics of S_N in the large system or *thermodynamic* limit, $N \to \infty$. Using Stirling's formula (Appendix A.1),

$$P\left(S_N = r\right) \sim \frac{1}{\sqrt{2\pi N r(1-r)}} e^{-NI(r)} \tag{2.3}$$

where

$$I(r) = \ln 2 + r \ln r + (1-r) \ln (1-r) \tag{2.4}$$

is independent of N at each fixed $r \in [0, 1]$ (Figure 2.2a).

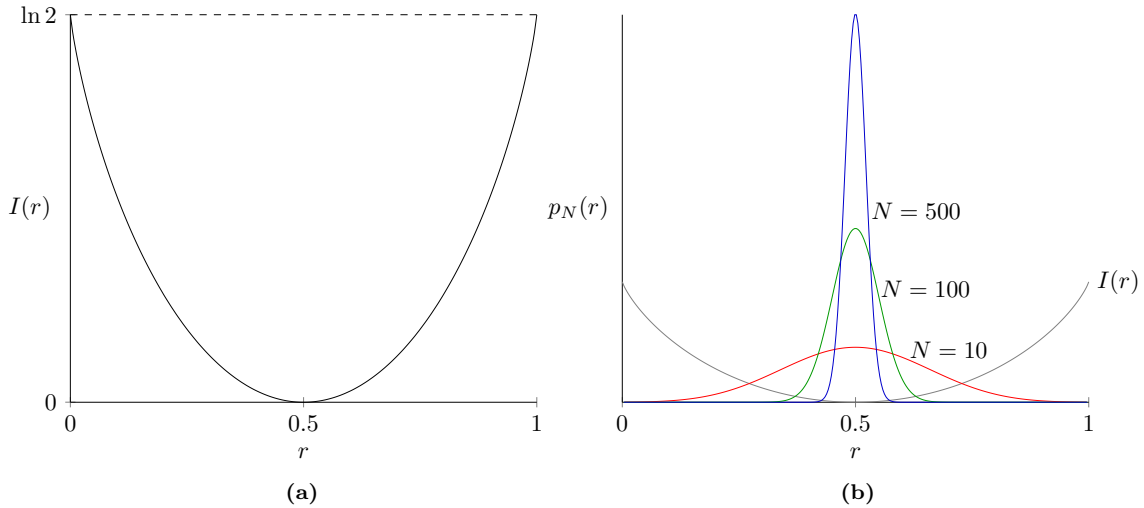

Figure 2.2: (a) Function controlling the exponential behaviour of the distribution of S_N and (b) the associated probability distribution (2.9) at $N = 10$, 100 and 500. Note that $I(r)$ is non-negative, strictly convex and has a single minimum at $1/2$ – the mean value of any one spin as well as the *expected* limiting value of S_N for large N (the law of large numbers).

In the same limit the rational values $r = k/N$ become dense in $[0, 1]$ and we can treat[1] S_N as a continuous random variable, introducing a probability *density* $p_N(r)$ via

$$P\left(S_N \in [r_1, r_2]\right) = \sum_{r_i \in [r_1, r_2]} P\left(S_N = r_i\right) \tag{2.5}$$

$$= \sum_{r_i \in [r_1, r_2]} NP\left(S_N = r_i\right) \Delta r_i \qquad (\Delta r_i = 1/N) \tag{2.6}$$

$$\underset{\Delta r_i \to 0}{\longrightarrow} \int_{r_1}^{r_2} p_N(r) dr \tag{2.7}$$

As such,

$$p_N(r) = NP\left(S_n = r\right) \sim \sqrt{\frac{N}{2\pi r(1-r)}} e^{-NI(r)} \tag{2.8}$$

It is instructive to plot $p_N(r)$ alongside $I(r)$ for different values of N (Figure 2.2b). We see that, as N increases, values away from $r = 1/2$, the unique minimum and zero of I, become exponentially unlikely. Put another way, as $N \to \infty$, only those configurations with $S_N \approx 1/2$ have a non-negligible probability of being observed in systems of random spins.

Large deviation theory follows the leading exponential behaviour, so in a final approximation we neglect the subdominant prefactor ($\ln N^{1/2} = o\left(N\right)$) to obtain

$$p_N(r) \sim e^{-NI(r)} \tag{2.9}$$

This is our first example of a large deviation approximation.

[1]Such treatment, often seen in physics, is mathematically justified by the weak convergence of S_N to a continuous random variable [13].

In general, if S_N is a random variable with parameter N and probability density $p_N(r)$, we say that S_N *obeys a large deviation principle* (LDP) if the limit

$$I(r) = \lim_{N\to\infty} -\frac{1}{N}\ln p_N(r) \tag{2.10}$$

exists. In this case we write

$$p_N(r) \asymp e^{-NI(r)} \tag{2.11}$$

the meaning of $\asymp$ being precisely that a relationship of the form (2.10) holds with $I(r)$ non-trivial.

$I(r)$ is known as the rate function or *rate* of the LDP and N its *speed.* The latter dictates how quickly p_N decays to zero with N; more generally, any positive sequence x_N such that $x_N \to \infty$ as $N \to \infty$ may multiply the rate function [12]. While of relevance to certain physical systems (see [14, 15] for recent examples), we will not encounter such LDPs. Indeed, the variables we take most interest in will be discrete random variables that converge in the above sense to continuous ones, with parameter and linear speed t (time).

2.1.2 Applicability

Before developing the theory surrounding the large deviation principle, we discuss its application in physical contexts through the analysis of *time-averaged observables.*[2] The motivation for studying these observables is that they encode both space *and* time correlations of a system and are hence capable of revealing information that instantaneous values cannot [16].

We consider the class of stochastic systems that at long times converge to a unique steady state. Let b be a dynamical observable in such a system, a quantity whose value $b = b(\mathcal{C}_t)$ at a time t depends on the configuration $\mathcal{C}_t$ of the system at that instant. In other words, as time proceeds C_t traces a trajectory upon which b varies. For instance, if each spin in the above system became a time-dependent random variable $\sigma_i = \sigma_i(t)$, then $\mathcal{C}$ would be the collection $(\sigma_1, \sigma_2, \ldots, \sigma_N)$ and $b = b(t)$ could again be the excitation density.

The *time-average* of b over an interval $[0, t]$ is

$$\bar{b}(t) := \frac{1}{t}\int_0^t b(\mathcal{C}_\tau)d\tau \tag{2.12}$$

Different trajectories give rise to different values of $\bar{b}$, so this average is itself a random variable. Suppose it was found to obey a large deviation principle; i.e., had a probability density $p_t(\bar{b})$ satisfying

$$p_t(\bar{b}) \asymp e^{-tI(\bar{b})} \tag{2.13}$$

with well-defined rate

$$I(\bar{b}) = -\lim_{t\to\infty}\frac{1}{t}\ln p_t(\bar{b}) \tag{2.14}$$

If $I(\bar{b})$ took the form of that in Figure 2.2a, with a unique zero at $\bar{b} = \langle b\rangle$ say, then, at long times t, $\bar{b}$ is exponentially unlikely to differ from $\langle b\rangle$. We recognise $\langle b\rangle$ as a mean, obtained from

[2] This is a main way in which large deviation theory is applied in physics. More generally, the theory provides a rigorous formulation of both equilibrium and non-equilibrium statistical mechanics i.e. a collection of techniques for calculating entropies and free energies. This is the formulation that was pioneered by Ellis [9] and is summarised by Touchette in his review [1].

the ensemble average

$$\langle b\rangle = \int b p_s(b) db \tag{2.15}$$

where $p_s(b)$ denotes the probability distribution in the steady state. This situation is the typical one in thermodynamics where physical systems are often taken to be *ergodic,* meaning that time-averaged measurements coincide with ensemble averages at long times. These measurements are usually found to obey a central limit theorem, being normally distributed about $\langle b\rangle$ with a variance that decays as t^{-1}. Assuredly, when $I(\bar{b})$ is analytic with a unique global minimum at $\langle b\rangle$, we have the Gaussian approximation

$$I(\bar{b}) \approx \frac{I''\left(\langle b\rangle\right)}{2}\left(\bar{b}-\langle b\rangle\right)^2 \rightarrow p_t(\bar{b}) \approx e^{-tI''(\langle b\rangle)\left(\bar{b}-\langle b\rangle\right)^2/2} \tag{2.16}$$

It can be shown [1] that is valid for deviations $(b-\langle b\rangle)$ of the order $O\left(t^{-1/2}\right)$ and

$$\frac{1}{tI''\left(\langle b\rangle\right)} = \frac{\sigma_b^2}{t} \tag{2.17}$$

where σ_b^2 is the variance of b. In other words, the large deviation principle offers the same description as the central limit theorem for small deviations of b. But through the full rate function it also captures large deviations in $\bar{b}$ for which the central limit theorem provides no useful information.

More interesting is the case when I does not take such a simple form. Then $\bar{b}$ may differ significantly from its mean value, even as $t \rightarrow \infty$ [2]. In light of (2.13), such events are considered *exponentially rare.* Thus large deviation theory enables us both to question whether time-averages converge to ensemble averages and to characterise rare events in the case that they do not. Ergodicity, or rather the breaking of it, will be a recurring theme in this essay. See [2] for a recent review on its importance in the study of physical systems with stochastic dynamics.

As mentioned in the introduction, we will be studying continuous time Markov chains. These describe systems that make *discrete* jumps between possible configurations at times $t_1, t_2, \ldots$ between which $\mathcal{C}_t$ is a constant. Consequently, the relevant dynamical observables will be of the form

$$\bar{a} = \frac{1}{t}\sum_{\mathcal{C}\rightarrow\mathcal{C}'} \alpha\left(\mathcal{C},\mathcal{C}'\right) \tag{2.18}$$

where α quantifies the change associated with the transition from $\mathcal{C}$ to $\mathcal{C}'$, and the sum runs over all transitions occurring in $[0,t]$. For example, $\mathcal{C}$ could be an atomic state and α the energy of the photon emitted following relaxation, in which case $\bar{a}$ records the average power emitted. An LDP for $\bar{a}$ is interpreted in the same way as one for a variable of type $\bar{b}$. Both types of averages are referred to as *additive processes,* the focus of a great number of large deviation analyses.

2.1.3 Calculating Rate Functions

In order to establish a LDP for a random variable $\bar{b}$, one can work directly with the probability density $p_t(\bar{b})$, bringing it to exponential form as was done for S_N above. However, an explicit expression for this density is rarely accessible. Instead, one must look to determine the rate function *indirectly.* A standard procedure for doing so is presented below.

It is firstly necessary to define the scaled cumulant generating function (SCGF),[3]

$$\psi(s) := \lim_{t\to\infty} \frac{1}{t} \ln \left\langle e^{-st\bar{b}} \right\rangle \tag{2.19}$$

which satisfies $\psi(0) = 0$ on account of normalisation ($\langle 1 \rangle = 1$). As the name suggests, ψ gives rise to scaled *cummulants* of $\bar{b}$. The mechanism? Repeated differentiation:

$$\psi'(0) = \lim_{t\to\infty} \left. \frac{\left\langle -\bar{b}e^{-st\bar{b}} \right\rangle}{\left\langle e^{-st\bar{b}} \right\rangle} \right|_{s=0} = -\lim_{t\to\infty} \left\langle \bar{b} \right\rangle, \tag{2.20}$$

$$\psi''(0) = \lim_{t\to\infty} t \left[\left\langle \bar{b}^2 \right\rangle - \left\langle \bar{b} \right\rangle^2 \right] = \lim_{t\to\infty} t \operatorname{Var}\left(\bar{b}\right) \tag{2.21}$$

and so on.

For the simple case when $\bar{b}$ obeys a central limit theorem with mean $\langle b \rangle$ and variance σ_b^2/t, the generated cumulants are seen to be those of b

$$\psi'(0) = -\langle b \rangle \quad \text{and} \quad \psi''(0) = \sigma_b^2 \tag{2.22}$$

In contrast to $I(\bar{b})$, which is everywhere non-negative,[4] $\psi(s)$ may take on both positive and negative values. Furthermore, a simple application of Hölder's inequality (Appendix A.2) demonstrates that $\psi(s)$ is always convex, a property not guaranteed for $I(\bar{b})$. Yet the two are intimately related, with knowledge of one allowing for calculation of the other. This leads us to the main result of this section:[5]

If $\psi(s)$ is differentiable, then $\bar{b}$ satisfies a large deviation principle

$$p_t(\bar{b}) \asymp e^{-tI(\bar{b})} \tag{2.23}$$

with rate function

$$I(b) = \psi^* := \sup_s \left[-sb - \psi(s)\right] \tag{2.24}$$

(To simplify the notation, in what follows b is used as the argument I instead of $\bar{b}$.)

The prescription $\psi \to \psi^*$ is known as the *Legendre-Fenchel transform* [17] which, for convex and differentiable ψ, reduces to the Legendre transform familiar from statistical physics [1]: the supremum of $-sb - \psi(s)$ either comes from $s = -\infty$, in which case $I = \infty$ and the decay is super-exponential, or a solution to

$$\left(sb + \psi(s)\right)' = 0 \to \psi'(s) = -b \tag{2.25}$$

If ψ is further *strictly* convex, this solution is unique and so defines a function $s(b)$ such that $\psi'\left(s(b)\right) = -b$, giving the standard form

$$I(b) = \psi^* \equiv -s(b)b - \psi\left(s(b)\right) \tag{2.26}$$

Moreover, $s(b)$ can be inverted to obtain a function $b(s)$ satisfying $b(s) = -\psi'(s)$. Then

$$I'(b) = -s'(b)b - s(b) - \psi'\left(s(b)\right)s'(b) \to I'\left(b(s)\right) = -s\left(b(s)\right) = -s \tag{2.27}$$

[3]Use of a negative rather than positive exponent here results in mildly inconvenient minus signs, but is the more natural choice in the context of statistical mechanics where, as we shall see, ψ takes the role of a free energy.

[4]One might worry about a negative value $I(b^*)$ arising from a singular distribution (e.g. δ_0), but this is in fact precluded by the rigorous definition of the LDP [9].

[5]Detailed discussion of this result, including its proof, is given by Touchette [1, Sec III.C., App. C].

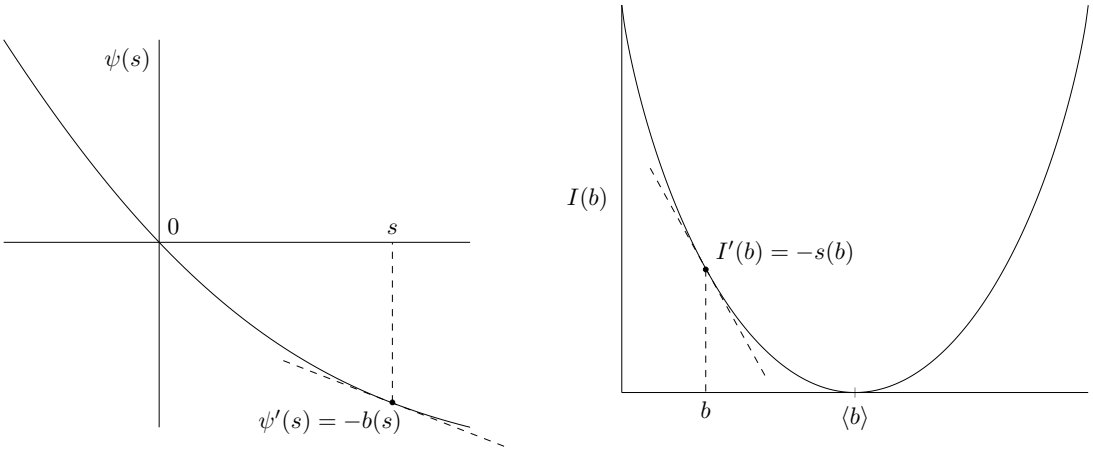

Figure 2.3: The SCGF and Legendre duality. The slope of $I(b)$ at b is the *negative* of the point at which the slope of $\psi(s)$ is $-b$. Note the negation: the behaviour of $\psi(s)$ for $s > 0$ relates to that of $I(b)$ for $b < \langle b \rangle$ and vice versa.

and $I'(b) = -s(b)$. Thus, the slopes of $\psi(s)$ and $I(b)$ have a one-one correspondence (Figure 2.3), a property known as *Legendre duality.*

Further geometric properties of the transform are developed in the following subsection. For now we state two important facts that will be useful later (see [17] or [18] for proofs):

i) The Legendre-Fenchel transform is self-inverse or *involutive* on the space of *closed*[6] convex functions i.e. $\psi^{**} \equiv \psi$ for ψ closed, convex

ii) When ψ is *strictly* convex and differentiable, $\psi^* \equiv I$ is too

As a simple example of the transform in action, we calculate the SCGF $\psi(s)$ for the system of independent spins considered above and rederive the rate function $I(r)$. Recall we had

$$S_N = \frac{1}{N} \sum_{i=1}^{N} \sigma_i \tag{2.28}$$

The SCGF for S_N is

$$\psi(s) = \lim_{N\to\infty} \frac{1}{N} \ln \left\langle e^{-sNS_N} \right\rangle = \lim_{N\to\infty} \frac{1}{N} \left\langle e^{-s\sum \sigma_i} \right\rangle \tag{2.29}$$

Since the σ_i are statistically independent and identically distributed,

$$\left\langle e^{-s\sum \sigma_i} \right\rangle = \sum_{i=1}^{N} \left\langle e^{-s\sigma_i} \right\rangle = N \left\langle e^{-s\sigma_i} \right\rangle \tag{2.30}$$

[6] $\psi : D \to \mathbb{R}$ is closed if $\{s \in D : \psi(s) \leq \alpha\}$ is a closed subset of $\mathbb{R}$ for each real α. Since convex functions are continuous on the interior of their domains, this is true if *iff* ψ is continuous at each boundary point in D and $\psi(s) \to \infty$ at each boundary point not in D [18].

where in the last average σ_i is any one of the summands. So

$$\psi(s) = \ln\left\langle e^{-s\sigma_i}\right\rangle \tag{2.31}$$

$$= \ln\left[P(\sigma_i = 0) + P(\sigma_i = 1)e^{-s}\right] \tag{2.32}$$

$$= \ln\left(1 + e^{-s}\right) - \ln 2 \tag{2.33}$$

This is the function plotted in Figure 2.3a. Being differentiable on $\mathbb{R}$, we know that S_N satisfies a LDP while

$$\psi'(s) = -r \to \frac{1}{1+e^s} = r \tag{2.34}$$

can be inverted for $r \in (0,1)$ to give

$$s(r) = \ln(1-r) - \ln r \tag{2.35}$$

and hence the rate function

$$I(r) = -s(r)r - \psi\left(s(r)\right) \tag{2.36}$$

$$= r\ln r - r\ln(1-r) - \left[\ln\left(1 + \frac{r}{1-r}\right) - \ln 2\right] \tag{2.37}$$

$$= \ln 2 + r\ln r + (1-r)\ln(1-r) \tag{2.38}$$

in agreement with (2.4).

Note that this method cannot be used to determine the rate function in all cases. In particular, the Legendre-Fenchel transform of a function is necessarily convex [17], so it can never be used to find a non-convex rate function. Large deviation theory provides other approaches to handle such cases, including a powerful *contraction principle* in which a rate function for $\bar{b}$ is calculated via its relation to a second random variable for which an LDP has already been established [1]. For our purposes recourse to the transform will always suffice.

2.1.4 Geometric Properties of the Legendre Transform

Our studies of kinetically constrained models (Section 3) will involve sequences of generating functions that, while individually analytic and strictly convex, have non-differentiable *limits* with linear parts. It will thus prove valuable to develop a geometric appreciation of the transform in cases more general than that of Figure 2.3.

To do so, we introduce the concept of *supporting lines* [18]. A function $f(s) : D \to \mathbb{R}$ is said to admit a supporting line at $r \in \mathbb{R}$ if there exists a $\lambda \in \mathbb{R}$ such that

$$f(s) - f(r) \geq \lambda(s - r) \quad \forall s \in D \tag{2.39}$$

This notion is illustrated in Figure 2.4. As should be graphically clear, supporting lines provide an equivalent formulation of convexity on open sets: f is convex on (s_0, s_1) if and only if it admits at least one supporting line at each $r \in (s_0, s_1)$ [18]. Moreover, if f is differentiable at r, then the tangent line at r provides a unique support. Supporting lines can be used to determine how non-differentiable points or linear parts of a convex function behave under a Legendre-Fenchel transform [19].

Refer to Figure 2.5a, where f is strictly convex but fails to be differentiable at $s = s_c$. At each point $(s, f(s))$ on the differentiable branches, f admits a unique supporting line with slope $f'(s) = -b$ – the tangent line. We have seen how such points are sent to pairs $(b, f^*(b))$ on the

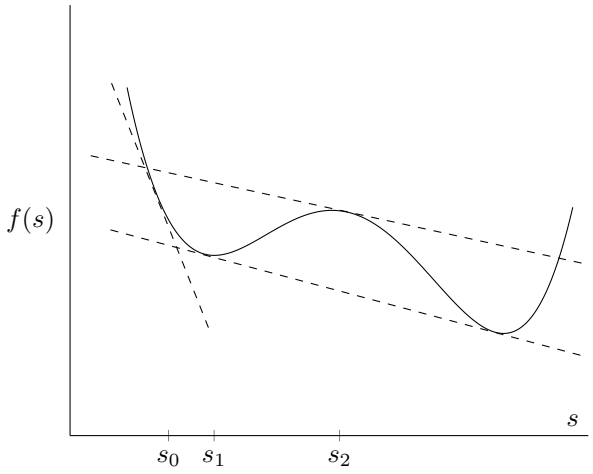

Figure 2.4: A supporting line of f is touches the graph of f at one or more points but otherwise lies below it. Here f has unique supporting lines at s_0 and s_1. The latter is said to be non-strictly supporting, since it touches the graph of f at a second point. The point s_2 admits *no* supporting lines, since f is non-convex there. After [19].

graph of the transform with support lines (tangents) of slope $(f^*)'(b) = -s$. This means that the differentiable branch **1** of f, with slopes ranging from $-\infty$ to $-b_l$, is mapped to the differentiable branch **1*** of f^* on $(+b_l, \infty)$. Similarly, $f'(s) \in (-b_r, \infty)$ on **2** so the corresponding branch of f^* covers $(-\infty, b_r)$.

At the non-differentiable point s_c, f admits *infinitely* many supporting lines with slopes in the range $[-b_l, -b_r]$. Consequently, at each $b \in [b_r, b_l]$ f^* must admit a supporting line of slope s_c [19]. The result is a *linear* branch. Since f here is closed, the transform is involutive ($(f^*)^* \equiv f$) and we can in the other direction and say that linear parts of a function are mapped to non-differentiable points under the transform, with left and right derivatives determined by the extent of the linear part.

Finally, these ideas can also be used to understand what happens at an end point of a differentiable branch, such as that of the function in Figure 2.6a. There the endpoint s_0 may be considered to admit supporting lines with slopes from $-\infty$ to 0, corresponding to a linear branch of slope s_0 on the graph of the transform.

2.2 The Glass Transition

In materials science, glass is a broad term including not on the familiar silicates (window glasses) but also many plastics, rubbers and ceramics. Common to these materials is the lack of an ordered crystalline structure (they are *amorphous*) and a quite generic transition that occurs in their formation.

We take this transition, the glass transition, to be the primary concept. In full generality, it is a change in a many-body system from an equilibrium fluid state to a non-equilibrium disordered solid [3]. A *glass former* is then any substance liable to such a transition. Molecular liquids offer a prototype, entering a glassy state when supercooled, but glass transitions are also observed in colloidal suspensions [20], granular material [21] and even dense living matter [22]. The diversity of this list and the range of length scales it encompasses only underscores the importance of the glass transition problem. For, despite extensive study, our understanding of the transition and

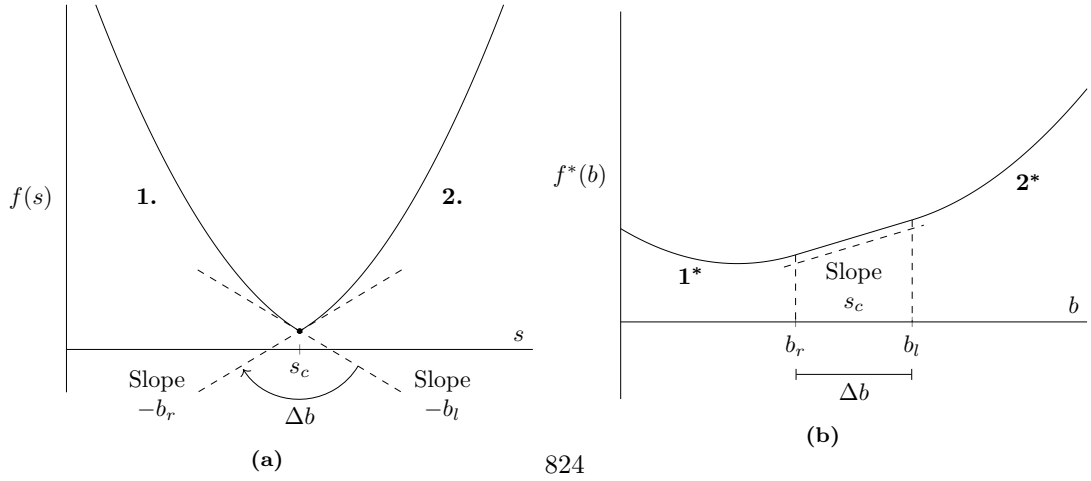

824

Figure 2.5: (a) A non-differentiable point $s = s_c$ of f conveys (b) a linear branch of slope s_c to f^*.

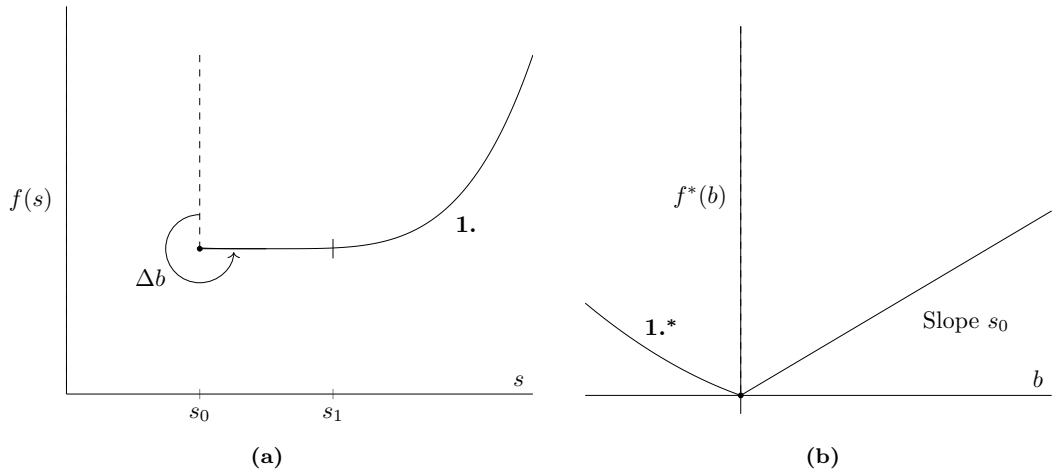

Figure 2.6: (a) Function defined on the interval $[s_0, \infty)$. (b) The closed endpoint conveys a linear branch over the positive real axis of f^*. Of course, that f^* has a non-differentiable point at 0 means that f is linear – constant in fact – on (s_0, s_1), where $-s_1$ is the left derivative of f^* at 0.

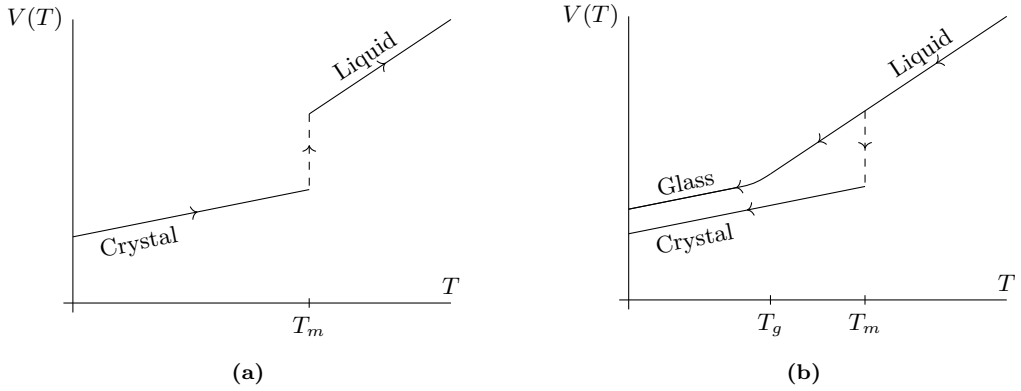

Figure 2.7: (a) Sketch of the heating and subsequent melting of a crystalline solid in the T-V plane. The crystal melts at $T = T_m$. (b) In the reverse direction, there are two possible outcomes. Slow cooling results in a crystal, rapid cooling a glass. In the latter case, the liquid must be brought through $T_g < T < T_m$ sufficiently quickly in order to bypass crystallisation. The continuity of the glass forming path reflects an essential feature of the process: slowdown without apparent structural change [3].

its physical origin is far from complete.

Theoretical approaches generally associate the glass transition with some underlying singular phenomenon and fall into one of two classes according to the *nature* of this singularity. In one approach, it is a conventional thermodynamic transition. Random first-order transition (RFOT) theory [23] is a prevailing example of this type. The perspective of the other class, and the one that we shall follow, is that transition has dynamical origins. This is the dynamical facilitation (DF) theory [24], of which kinetically constrained models are the basis.

Certainly, the nature of the transition and its driving mechanisms are the fundamental issues. Yet any complete theory should able to account for all empirical observations, and in a coherent way. In this section we present the main phenomenology and its relation to the dynamic theory. We begin with an overview of the glass formation process.

2.2.1 Glass Formation Versus Crystallisation

Figure 2.7a is a plot of volume against temperature for a typical crystalline solid undergoing steady heating. As temperature is increased the molecules comprising the crystal, initially held rigidly in place by permanent bonds with their neighbours, become increasing agitated. Their oscillations, and so mean separation, increases; the solid expands. Eventually, they acquire enough energy to break free of the immediate confines of their neighbours and melting ensues. This is marked by a vertical section since energy (latent heat) must be supplied in order to melt a solid already at its melting point, both on account of the increased potential energy of the molecules in the liquid phase and the greater volume of that phase. Going in the opposite direction we have freezing or, more specifically, *crystallisation:* molecular energy decreases, the liquid contracts, a crystal forms. A second possibility exists for the solid state, however.

Crystallisation does not take place instantaneously, being impeded by the finite viscosity of the fluid and associated molecular relaxation timescale τ. The latter characterises the time over which the molecular structure can reconfigure and increases dramatically as the liquid is cooled. It follows that, if a sample is called sufficiently rapidly, its molecules may be brought to an

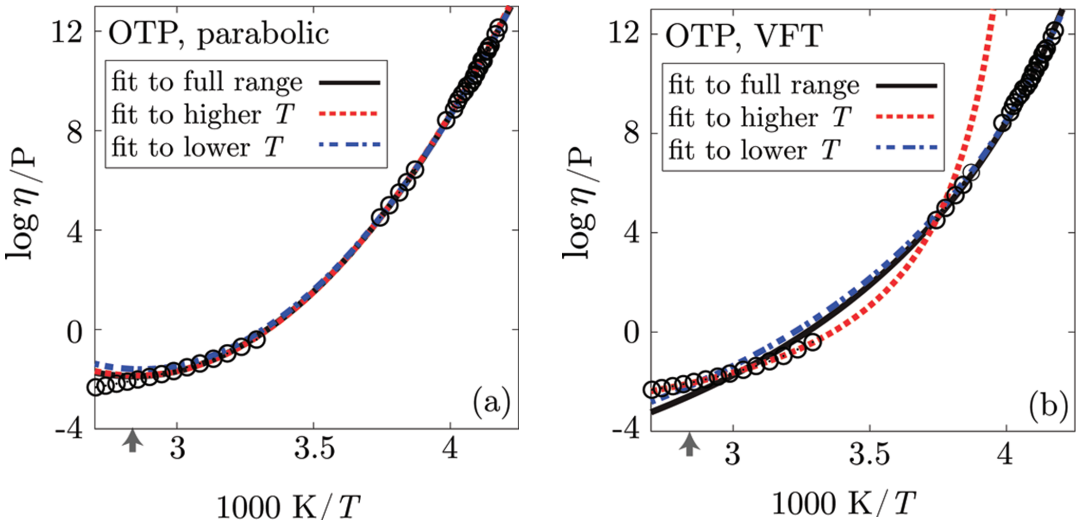

Figure 2.8: Logarithm of viscosity η (Poise, 1P = 0.1Pa·s) as a function of inverse temperature for the organic liquid OTP (ortho-therphenyl) [26]. For both (a) the parabolic form (2.42) and (b) the VFT law (2.41) three fits are provided. These minimise the mean square deviation from experimental data [27] (circles) for either the lower, higher or complete temperature range of data. The parameters J, T_0 of (2.42) were found to be largely independent of the chosen temperature range. This was not the case for the VFT law which does not offer reliable predictions outside of the interval over which it was fit. Reprinted with permission from [26]. Copyright 2020 American Chemical Society.

effective half *before* crystallisation[7] has chance to occur. Hence the principle of glass formation: supercool a liquid to a temperature T_g at which τ exceeds any reasonable observation time.[8] As the liquid loses its ability to undergo changes in molecular configuration, disorder present prior to the transition is 'frozen in,' producing an amorphous solid i.e. a glass. The crystalline phase still offers the thermodynamic state of lowest free energy [4], only this is rendered – kinetically – inaccessible. It is in this sense that the glass transition is one between an equilibrium fluid state and a *non-equilibrium* solid one. As we will see below, τ diverges with decreasing temperature. This signals the loss of ergodicity of the fluid state, a property that relies on the system exploring its configuration space over experimentally finite timescales.

While supercooled liquids provide a simple example, that the glass transition occurs in many other types of systems should be emphasised. The particular details vary, but the underlying principles, viz. slowdown and kinematic arrest, are the same regardless of whether the system comprises molecules in a liquid, a suspension of particles (colloid) or granular material. In fact virtually any material can, *if cooled fast and long enough,* be prepared as an amorphous solid [4]. The basic requirement appears to be some form of local excluded volume interactions [3]. *How fast* and *how long* of course depends on the material. For 'good' glass former such as Silica (SiO_2, $T_g = 1430$K), cooling rates $\sim 10^{-4}$–10^{-1}Ks^{-1} typically suffice, whereas metallic alloys (e.g. Au_8Si_2, $T_g = 290$K) may require rates many order of magnitudes higher [4].

2.2.2 Structural Relaxation

We have now seen how the glass transition occurs when the characteristic time τ of molecular motions becomes exceptionally large, prohibiting structural rearrangement. The changing timescale τ, in particular its temperature dependence, is central to the glass transition problem and indeed any study of slow dynamics.

In a general setting, *relaxation* refers to any process in which a system responds to a perturbation in the form of some external input or parameter change [28]. It is a time-dependent change *towards* equilibrium. This encompasses a broad range of processes depending on whether the stress be mechanical, electrical, chemical or of a thermodynamic kind (e.g. a change in temperature). The decaying response is described by autocorrelation or relaxation functions which in many cases assume an exponential form. A simple example is the stress relaxation function, $\Psi(t) := G(t)/G(0)$. Here $G(t)$ is the shear modulus (ratio of stress to strain) of a sample in a stress relaxation experiment. According to the Maxwell model (Appendix B.1),

$$\Psi(t) = e^{-t/\tau_s} \tag{2.40}$$

where τ_s is the stress relaxation time such that $\Psi(\tau_s) = 1/e$. For $t \ll \tau_s$, the system has not had time to respond and $\Psi(t) \approx 1$. At long times $t \gg \tau_s$ $\Psi(t) \approx 0$ is again unchanging, the response having long decayed away. It is only for times $t \sim \tau_s$ that significant change is recorded.

For glass formers, the aim is to assess timescales of *structural relaxation,* since these fundamentally determine whether the material behaves as a liquid, with the ability to respond and change shape, or a solid. Dielectric, orientational and mechanical relaxation timescales are all frequently measured for this purpose [29]. In addition, macroscopic transport properties such as viscosity and diffusivity as well as microscopic observables such as the density-density correlation function $\langle Q(t) \rangle$ (Appendix B.2) are studied. Changes in these quantities as the transition is approached manifest those of the underlying timescale τ (for example, the viscosity $\eta \propto \tau$ – see Appendix B). Broadly, there are two key observations.

The first is that behaviour is not quite exponential in time. Instead, the final decay of most correlation functions takes a *stretched* exponential form $\propto e^{-(t/\tau)^b}$ with $b \in (0, 1)$, a function often seen in the analysis of relaxation and diffusion in complex systems [28]. The second, which we focus on, concerns the *temperature dependence* of the relaxation timescales. Not only do these diverge with decreasing temperature, but they do so faster that exponential in inverse temperature. This is known as *super-Arrhenius* behaviour in reference to the Arrhenius law $\propto e^{-A/k_B T}$ prevalent in the field of chemical kinetics [30].

Many functional forms have been proposed for $\tau = \tau(T)$ [29]. The Vogel-Fulcher-Tammann (VFT) law is historically a popular one:

$$\tau = \tau_0 e^{A/(T - T_{\mathrm{VFT}})} \tag{2.41}$$

where A and T_{VFT} are fitting parameters. This form may be reasoned within the framework of RFOT theory, the divergence at T_{VFT} a precursor of the predicted thermodynamic transition. On the other hand, DF theory prescribes a parabolic exponent [24],

$$\tau = \tau_0 e^{J^2 (T_0 - T)^2 / T^2} \qquad (T < T_0) \tag{2.42}$$

which is singular at $T = 0$ only. Again, J and T_0 are fit to the data. The latter temperature is indicative of the boundary between the normal and supercooled regimes [26].

[7] Shelby [25, Ch. 2] covers kinetic theories for nucleation and crystal growth. We do not discuss these processes as it is structural relaxation (Section 2.2.2) that fundamentally characterises glassy behaviour.

[8] $\tau \sim 100$s is often taken to define T_g [3]. In practice its final value will be far greater (upwards of 10^{10}yr [4]).

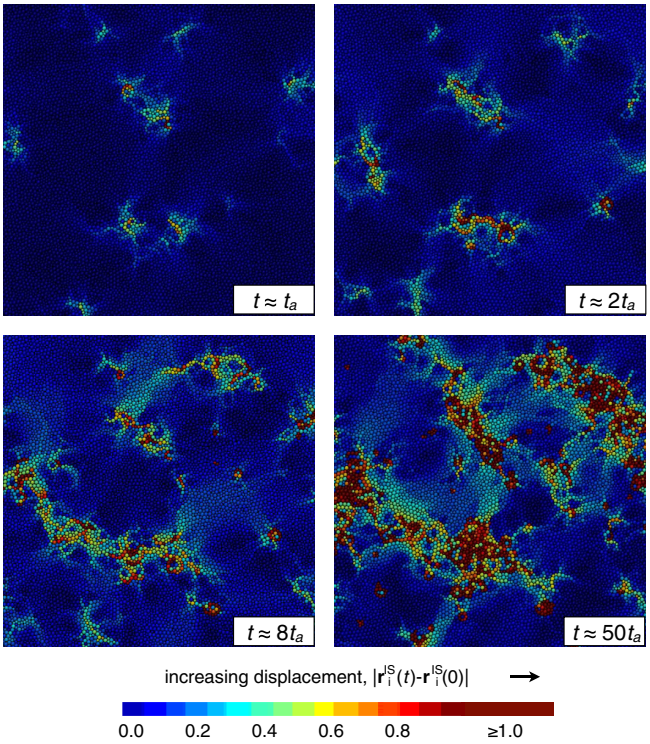

Figure 2.9: Dynamic Heterogeneity. Time evolution of particle displacements in an atomistic model of a glass former in the supercooled regime, from [32]. Particle motions become correlated, with regions of high mobility (red) growing outward. These regions connect on a timescale of the structural relaxation time $\tau \sim 500t_a$. Video of the simulation is available on the publisher's website (licensed under CC BY 3.0).

Figure 2.8 shows the logarithm of both functions fitted to viscosity data [27] ($\eta \propto \tau$) for the organic liquid OTP (ortho-therphenyl), from [26]. The authors favoured the use of the parabolic relationship on the grounds that the parameters J and T_0 appeared to be material properties independent of the range of experimental data considered, which was not the case for the VFT law. Yet more generally, both functions are found to fit measurements from supercooled liquids reasonably well, indicating that at an empirical level there is little to distinguish between the two approaches [3]. At any rate, they illustrate the severity of slowdown in a typical glass former as $T \to T_g^+$: transport properties can change upwards of 15 orders of magnitude for only a 3 or 4-fold reduction in temperature [31].

2.2.3 Dynamic Heterogeneity

The appeal of DF theory is its inherent ability to account for the phenomenon of *dynamic heterogeneity.* Relaxation is *not* uniform in space or time. Instead, a large distribution of relaxation timescales are observed in the glass former [3]. The physical picture is of slowly moving regions punctured by clusters of relatively mobile particles (Figure 2.9). This spatial clustering conveys inhomogeneity to density, viscosity and other transport quantities. It is in stark contrast to the situation in a high temperature liquid where one patch of fluid is essentially indistinguishable from any other and representative of the whole. Derivations of transport coefficients and their

relations are often based on this homogeneity, so it is unsurprising that many of these relations cease to apply for supercooled liquids [3].

While relaxation is studied by means of two-point functions (autocorrelators), correlations between relaxation processes are probed using *four-point* functions. The main example is the dynamic susceptibility χ_4, the four-point function associated with the density-density correlator $\langle Q(t)\rangle$ mentioned above. The precise relation between the two is described in Appendix B.2. Here we note that much effort has been done to characterising these functions and the dynamic correlations they reveal so as to better understand, for example, the changing length scales in dynamic heterogeneity [33]. Work here is led by numerical simulations since direct measurements, if possible, are often challenging [3].

Inextricably linked to heterogeneity in DF theory is the notion of *dynamic facilitation.* This describes how the relaxation motion of a localised region in the glass former gives rise to relaxation in a neighbouring region. This dynamical process underlies the behaviour of the kinetically constrained models we study in the next section. In analogy with the phenomena from quantum optics, it leads to *bunching* where one relaxation event is typically followed by many others [3]. It also provides insight into the breakdown of classical transport relations in the fluid, since these typically require independence of moving units [28]. While dynamic facilitation offers a driving mechanism for glass formation, proving that it is the dominant one is not straightforward: in a real liquid exchanges which lead to relaxation are tied up with motions that do not [3].

3 Kinetically Constrained Models

Kinetically constrained models (KCMs) are stochastic models of glass formers and the basis of dynamic facilitation theory. With only simple thermodynamics and local kinematic constraints, their purpose is to investigate whether the glass transition can be understood in terms of dynamical phenomena alone. We will find evidence that this is this case, reasoning in particular the role of the dynamical analogue of a first-order phase transition.

This section begins with an introduction to two extensively studied KCMs, the Fredrickson-Andersen (FA) and East models. The relaxation dynamics of both models and their correspondence with glass formers is discussed. Next, tools to study their dynamics are assembled, putting to use the large deviation machinery set out in Section 2.1. The main result of this section – the occurrence of dynamical phase transitions in the models – is then established. This result was first shown by Garrahan et al. in a 2007 letter [34] and expanded upon in an article by the same group [5] two years later. Finally, implications of the transition and the associated phase coexistence phenomena are examined.

3.1 Models of Glass Formers

3.1.1 The FA and East Models

Recall from Section 2 the line of N random binary variables or independent spins $n_i = 0,\ 1$. There we took $N \to \infty$, but for now we consider finite systems.[9] The first step is to add a dynamic character. Each site is taken to be a two level system with energy $n_i J$ and Boltzmann statistics

$$P(n_i) = \frac{e^{-n_i J/k_B T}}{Z} \tag{3.1}$$

[9]It will be important (Section 3.3.2) that we take the long-time limit ($t \to \infty$) before $N \to \infty$.

where $Z = \sum_{n_i=0}^{1} e^{-n_i J/T}$ is the one spin partition function. It is convenient to work in units of scaled inverse temperature $\beta = J/k_B T$ in terms of which

$$P(n_i) = \frac{e^{-\beta}}{Z} \tag{3.2}$$

On account of their independence, the distribution for a chain of N spins is

$$P_{\rm eq}(\{n_i\}) = \frac{1}{Z^N} \prod_i \frac{e^{-n_i\beta}}{1+e^{-\beta}} \tag{3.3}$$

and the mean excitation density c is just the expected value of any one of the n_i:

$$c := \langle n_i \rangle = \sum_{n_i=0}^{1} n_i P(n_i) = \frac{e^{-\beta}}{Z} \tag{3.4}$$

Note that c is a number between 0 ($k_B T \ll J$) and 1/2 ($k_B T \gg J$).

From here constrained models are obtained via a prescription of *rules* for which sites (spins) can change states. These typically have a *local* character: the behaviour of a given spin depends on the state of it nearest neighbours only. In the Fredrickson-Andersen (FA) model [35], only those spins with an excited neighbour can change state. Specifically, in one dimension all processes are forbidden *except* those of the form

Process	Rate
$10 \to 11$, $01 \to 11$	c
$11 \to 10$, $11 \to 01$	$1-c$

(3.5)

We take the chain to be periodic, so that the $N^{\rm th}$ spin may facilitate change in the first and vice versa, and do not double the rates in the case of two excited neighbours.

The extension of these rules to 2 and 3 dimensional lattices, or any regular graph for that matter, is the obvious one: excitation of a neighbour is facilitated at rate c, relaxation at $1-c$. These rates are chosen for reversibility in the sense that, for example

$$\frac{10 \to 11}{11 \to 10} = \frac{c}{1-c} = \frac{e^{-\beta}}{(1+e^{-\beta})-e^{-\beta}} = e^{-\beta} \equiv e^{-\Delta E/T} \tag{3.6}$$

where ΔE is the change in energy associated with the additional excitation. This ensures that the system obeys *detailed balance*[10] with respect to $P_{\rm eq}$ in (3.3). Hence we expect this distribution to describe long-time, steady state behaviour.[11] This will be crucial to the proof of the dynamical phase transition.

While the one-dimensional FA model exhibits stretched exponential relaxation behaviour, it does so with timescales τ_α that scale exponentially with $1/T$ only (see below). For *super*-Arrhenius behaviour, stronger constraints are required. This leads us to introduce the East model, where facilitation is restricted to a single direction only. The permissible transitions are then

Process	Rate
$10 \to 11$	c
$11 \to 10$	$1-c$

(3.7)

which also obey detailed balance with respect to (3.3). As before, the generalisation to higher dimensions is straightforward (Figure 3.1).

[10] Recall this is a statement of microscopic reversibility at equilibrium: the probability of observing a transition from configuration $\mathcal{C}$ to $\mathcal{C}'$ must balance that from $\mathcal{C}'$ to $\mathcal{C}$, since that is what 'at equilibrium' means. Note that this is not the same as saying the rate of transition is the same in both directions.

[11] In fact, in order to meet this expectation an additional condition is required: irreducibility (Section 3.2.1).

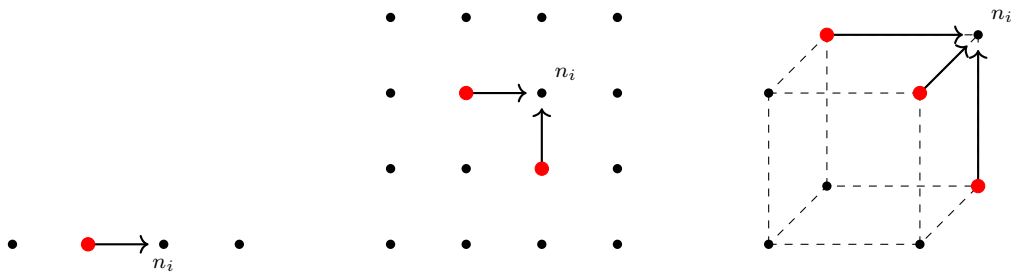

Figure 3.1: Neighbours (red) that can promote excitation or relaxation of the site labelled n_i in one, two and three-dimensional variants of the East model. *Caveat emptor.* The model's name is not indicative of the facilitated direction in $d > 1$!

3.1.2 Dynamical Correspondence and Relaxation Timescales

A pertinent question is in exactly what sense do KCMs model a glass forming liquid. A direct connection can be made by considering a coarse graining of the liquid to the order of several particle diameters [36]. Assigning a lattice site to each small region of fluid, a value $n_i = 1$ ($n_i = 0$) is then taken to indicate a density below (resp. above) some threshold at which molecular rearrangement can occur.[12] This establishes a correspondence between the diffusion of excitations in the models and that of mobile, low density regions in the glass former. Evidently, dynamics with pervading 0s are indicative of non-ergodic, glass-like phases. For the one-dimensional FA model, a simple argument may be used to estimate the *timescale* of this diffusion [16]:

In order for an isolated excitation to move one unit to the right, it must facilitate the excitation of its neighbour $\sim c$ and subsequently relax $\sim (1-c)$. Hence diffusion occurs at a rate $D \sim c(1-c) \sim c$ for $c \ll 1/2$ (low temperatures) where D is the diffusion coefficient. On dimensional grounds, this scales as $D \sim \ell^2/\tau_\alpha$ where ℓ is the typical separation of excitations and τ_α the relaxation time. Recalling that c is the equilibrium excitation *density,* under these conditions $\ell = c^{-1}$ and

$$\tau_\alpha \sim \frac{\ell^2}{D} \sim c^{-3} \sim e^{3\beta} \tag{3.8}$$

Since this argument required facilitation in both directions, it doesn't apply to the East model. Instead more convoluted diffusion pathways must be considered [16]. The upshot is that the more restrictive rules lead to an even greater separation of timescales; a rigorous result for the low temperature scaling is [37]

$$\tau_\alpha \sim e^{a\beta^2(1+o(1))} \tag{3.9}$$

with $a = (2\ln 2)^{-1}$. This is in the parabolic form (2.42) introduced in the previous section (T is low so $J^2/T^2 \gg J^2/T$). There we also described responses of stretched exponential form $e^{-(t/\tau)^b}$ ($b \in (0,1)$) and indeed this behaviour is found in many KCMs [38], including the one-dimensional FA and East models. It appears, quite surprisingly, that only basic kinetic constraints are sufficient to to produce glass-like relaxation.

[12] The reverse convention ($n_i = 0$ low mobility, $n_i = 1$ high mobility) is also seen in the literature [36]. In atomistic simulations, one may consider excitations to be large particle displacements [32], such as those handled by the correlator $\langle Q(t)\rangle$ (Appendix B.2).

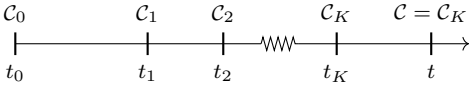

Figure 3.2: Over a period $[0, t]$ the system transitions $\mathcal{C}_0 \to \mathcal{C}_1$, $\mathcal{C}_1 \to \mathcal{C}_2$,... between accessible configurations to arrive in configuration $\mathcal{C}_K$. This defines a history $(\mathcal{C}_0, t_0)$, $(\mathcal{C}_1, t_1)$,..., $(\mathcal{C}_K, t_K)$. After [5].

3.1.3 Other Models

We have introduced the FA and East models as simple examples and it is with reference to these models that statistical tools and ultimately the result of the dynamical phase transition will be established. Yet aspects of their relaxation behaviour are common to a large class[13] of KCMs for which the result applies. This includes facilitated lattice gas models, such as the KA [39] and (2)-TLG models [40], where *particles* attempt to move between sites at a constant rate but are blocked if those sites are occupied; a more direct realisation of the excluded volume interactions in a glass forming liquid.

In addition, bosonic and mean-field variants of KCMs may be considered. These are obtained by allowing, in turn, n_i to take values greater than one and for facilitation to occur over any distance. Their utility comes when performing quantitative analysis as explicit forms of large deviation functions may be inaccessible in the original models but accessible in the variants.

3.2 Statistics Over Histories

The dynamics of the FA and East models describe continuous-time Markov chains: over the course of time the system makes a series of transitions or *jumps* $\mathcal{C}_0 \to \mathcal{C}_1$, $\mathcal{C}_1 \to \mathcal{C}_2$... between configurations $\mathcal{C} = \{n_i\}$ as excitations are created or lost. The sequence $\mathcal{C}_0, \mathcal{C}_1, \ldots, \mathcal{C}_K$ together with the associated jump times $t_1, \ldots, t_K$ defines a trajectory or *history* of length t (Figure 3.2) [5]. Since each site attempts to change state at a constant rate, one has exponentially distributed wait times between jumps and the probability $P(\mathcal{C}, t)$ of the system being in configuration $\mathcal{C}$ at time t evolves according to the *master equation*[14]

$$\partial_t P(\mathcal{C}, t) = -r(\mathcal{C}) P(\mathcal{C}, t) + \sum_{\mathcal{C}'} W(\mathcal{C}' \to \mathcal{C}) P(\mathcal{C}', t) \tag{3.10}$$

where $W(\mathcal{C}' \to \mathcal{C})$ is the rate of transitions from $\mathcal{C}'$ to $\mathcal{C}$ and

$$r(\mathcal{C}) := \sum_{\mathcal{C}'} W(\mathcal{C} \to \mathcal{C}') \tag{3.11}$$

is the escape rate from $\mathcal{C}$ (note $W(\mathcal{C} \to \mathcal{C}) = 0$). Relating back to the discussion above, for $\mathcal{C} = \{n_i\}$ we have $W(\mathcal{C} \to \mathcal{C}') = c$, $1 - c$ or 0 whilst detailed balance is the statement

$$P_{\text{eq}}(\mathcal{C}) W(\mathcal{C} \to \mathcal{C}') = P_{\text{eq}}(\mathcal{C}') W(\mathcal{C}' \to \mathcal{C}) \tag{3.12}$$

To make these notions more concrete, refer to Figure 3.3 which depicts example trajectories for a system of independent spins as well as the FA and East models at a temperature $T = J/2$. Note

[13] For a classification of the different types of KCMs, see the 2010 review by Garrahan et al. [36].

[14] The standard reference for stochastic methods in the sciences is the book by Gardiner [41, Ch. 3, 11]. Regardless, (3.10) is intuitive: the probability of being in $\mathcal{C}$ *decreases* according to the sum of all possible ways of leaving $\mathcal{C}$ whilst *increasing* according the weighted sum of possible transitions to $\mathcal{C}$ from another configuration $\mathcal{C}'$.

that although samples were taken at integer times $t = 0, 1, 2, \ldots$ between these many transitions typically occurred; a history records *every* transition. The other important consideration is the starting configuration $\mathcal{C}_0$. For the trajectories in Figure 3.3, a random configuration in which *half* of all sites were initially excited was chosen, simulating a quench from high temperatures ($T \gg J \to c \sim .5$). In general, an initial probability distribution $p_0(\mathcal{C}_0)$ is prescribed.

3.2.1 The Activity and Ensembles of Trajectories

While classical thermodynamics deals with probability distributions over the configurations of a large system, our interests lie in probability distributions *over histories.* It is therefore appropriate to construct a framework analogous to that of thermodynamics for handling ensembles of trajectories.

First, we need to define a suitable dynamic observable to study on the trajectories. Given the nature of the glass problem, this should capture the 'activity' (number of relaxation events) of a history $\mathcal{C}_0, \ldots \mathcal{C}_K$ [5]. The simplest measure, which we take to define the activity A, is the total number of jumps that occur in the history. This may be written $A = tN\bar{a}$ in terms of the additive process (cf. (2.18))

$$\bar{a} = \frac{1}{Nt} \sum_{k=0}^{K-1} \alpha(\mathcal{C}_k, \mathcal{C}_{k+1}) \quad \text{with} \quad \alpha(\mathcal{C}, \mathcal{C}') = 1 \; \forall \, \mathcal{C}, \mathcal{C}' \tag{3.13}$$

which is the activity density per unit time, an intensive quantity. According to the correspondence discussed above, A is representative of mobility throughout the liquid over an observation time t. Rare histories which are more or less active (mobile) than average are then characterised by the large deviations of A. As examples, the trajectories shown in Figure 3.3a, (b) and (c) had activities of 13068, 4855 and 2946 respectively.

In line with (2.19), we define the SCGF

$$\psi(s) = \lim_{t\to\infty} \frac{1}{t} \ln \left\langle e^{-stN\bar{a}} \right\rangle = \lim_{t\to\infty} \frac{1}{t} \ln \left\langle e^{-sA} \right\rangle \tag{3.14}$$

where $\langle \cdot \rangle$ now denotes an average over the ensemble of histories.

As in Section 2.1, implicit here is the assumption of long-time convergence to a steady-state, meaning that the associated Markov processes possess a unique limiting stationary distribution, namely P_{eq}. This is the case provided that, in addition to satisfying the property of detailed balance (3.12), the dynamics are *irreducible* i.e. every configuration is accessible from any other [38]. This is not immediately true for the FA and East models: the configuration with no excitations (all zeroes) is separated from the rest. While somewhat of a technicality, for the purpose of rigorous analysis we should therefore exclude these states e.g. choosing an initial distribution $p_0(\mathcal{C})$ that does not feature them. It is also known [1] that under these conditions (an additive process on a finite, irreducible chain) $\psi(s)$ is strictly convex and differentiable. Therefore $\bar{a} = A/Nt$ satisfies a LDP with rate function $I = \psi^*$ that is itself strictly convex and differentiable.

We now introduce the *s-ensemble* by weighting the probability of each history according to

$$P[\text{hist}] \to P[\text{hist}] \frac{e^{-sA[\text{hist}]}}{Z_A(s,t)} \tag{3.15}$$

where

$$Z_A(s,t) = \sum_{\text{hist}} P[\text{hist}] \, e^{-sA[\text{hist}]} \equiv \left\langle e^{-sA} \right\rangle \tag{3.16}$$

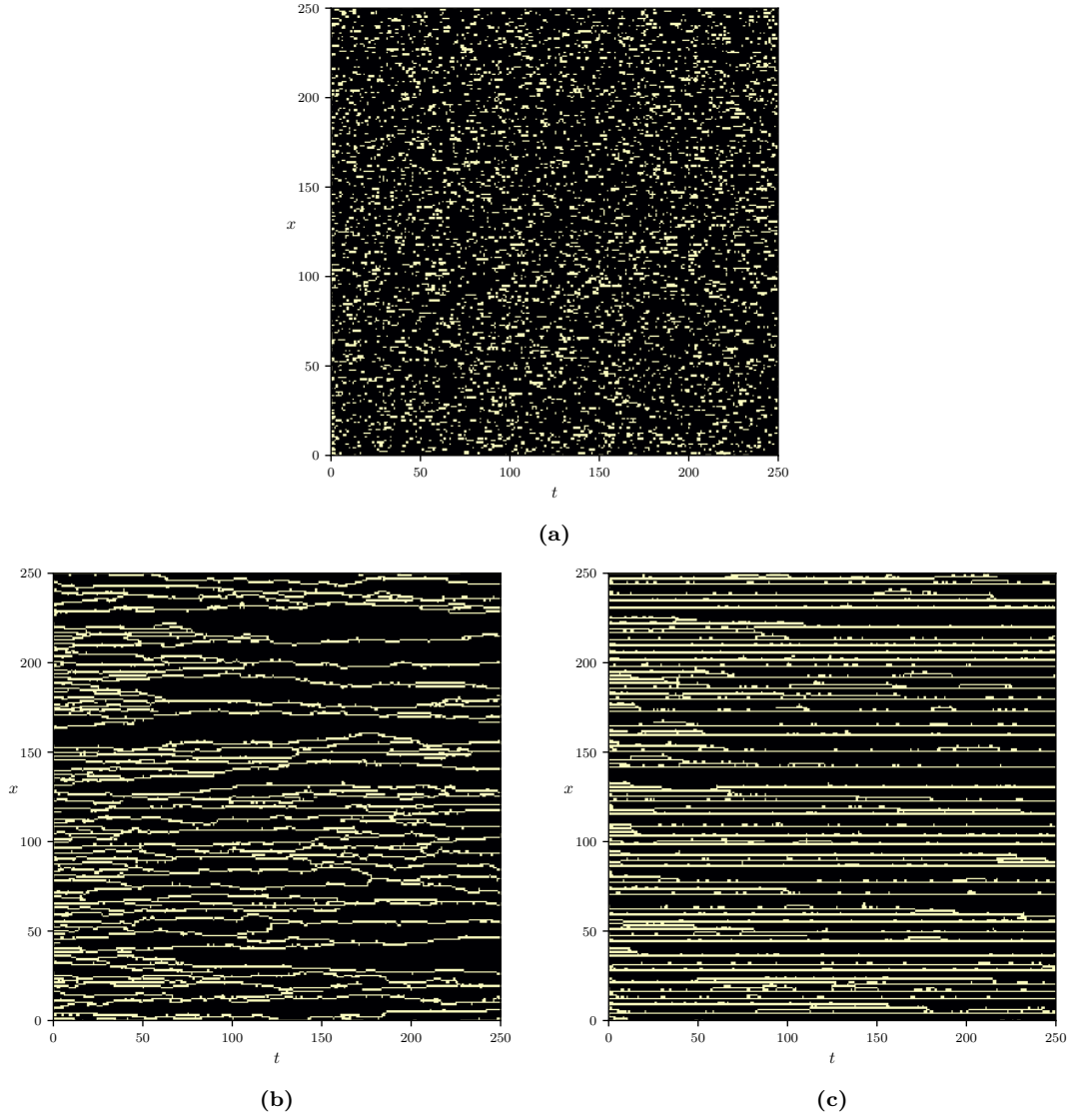

Figure 3.3: Example trajectories for (a) a system of independent spins, (b) the FA model and (c) the East model following a quench from high temperatures ($T \gg J$) to $T = J/2$. In each case 250 lattice sites (x coordinate) were simulated for an equal length of time (a light guide to simulating KCMs is given in Appendix C). Bright pixels correspond to an excitation, dark pixels the absence of one. The lack of correlations in (a) gives rise to a seemingly random collection of dots - no quench effects are visible as the system relaxes over a time $O(1/c) \sim 1$. In contrast, excitations in the FA model diffuse, branch and coalesce. Relaxation in the East model is even more restricted, with excitations moving in a single direction only (here vertical). Own work.

fixes the normalisation. The average of any history dependent observable O in the new ensemble is then given by

$$\langle O \rangle_s = \frac{\langle O e^{-sA} \rangle}{\langle e^{-sA} \rangle} \tag{3.17}$$

The s-ensemble is a convenient tool for accessing the large deviations of A. It is analogous to working with a family of Boltzmann distributions in the canonical ensemble, with s a field conjugate to A. The analogy is well summarised by [2, Sec. 2]. Here we note that biasing trajectories according to the value of A favours more ($s < 0$) or less ($s > 0$) active histories. The original ensemble and hence the true (physically accessible) steady-state averages of the system are recovered with $s = 0$ [5].

Appropriate to this analogy, we call $Z_A(s,t)$ the dynamical partition function and $\psi(s)$ the long-time limit of the *dynamical free energy* per unit time. The two are related by

$$\psi(s) = \lim_{t\to\infty} \frac{1}{t} \ln Z_A(s,t) \quad \text{or} \quad Z_A(s,t) \sim e^{t\psi(s)} \quad \text{at long times} \tag{3.18}$$

The efficacy of the s-ensemble comes from the fact that large deviation problems can be formulated as *eigenproblems* of operators on the space of configurations $\{\mathcal{C}\}$ [2]. To do so here, introduce the probability $P(\mathcal{C}, t|A)$ conditioned on the value of A at t and the generating function

$$P_A(\mathcal{C}, s, t) = \sum_{A=0}^{\infty} e^{-sA} P(\mathcal{C}, t|A) \tag{3.19}$$

This is just the component of Z_A associated with those histories reaching $\mathcal{C}$ at a time t:

$$Z_A(s,t) = \sum_{\mathcal{C}} \sum_{A} e^{-sA} P(\mathcal{C}, t|A) = \sum_{\mathcal{C}} P_A(\mathcal{C}, s, t) \tag{3.20}$$

Noting that A is incremented upon every configuration change, from (3.10)

$$\partial_t P(\mathcal{C}, t|A) = -r(\mathcal{C}) P(\mathcal{C}, t|A) + \sum_{\mathcal{C}'} W(\mathcal{C}' \to \mathcal{C}) P(\mathcal{C}', t|A-1) \tag{3.21}$$

and so the master equation for $P_A(\mathcal{C}, s, t)$ is

$$\partial_t P_A(\mathcal{C}, s, t) = -r(\mathcal{C}) P_A(\mathcal{C}, s, t) + \sum_{\mathcal{C}'} e^{-s} W(\mathcal{C}' \to \mathcal{C}) P_A(\mathcal{C}', s, t) \tag{3.22}$$

Borrowing bra-ket notation from quantum mechanics, we set up an abstract finite vector space of configurations $|\mathcal{C}\rangle$ with inner product $\langle \mathcal{C}|\mathcal{C}'\rangle = \delta_{\mathcal{C}\mathcal{C}'}$ and take the vector $|P(s,t)\rangle = \sum_{\mathcal{C}} P_A(\mathcal{C}, s, t)\,|\mathcal{C}\rangle$ to represent the state of the system at time t. Defining an operator $\widehat{W}$ on this space with matrix elements

$$W_{\mathcal{C}\mathcal{C}'} = \langle \mathcal{C}|\widehat{W}|\mathcal{C}'\rangle = e^{-s} W(\mathcal{C}' \to \mathcal{C}) - r(\mathcal{C}) \delta_{\mathcal{C}\mathcal{C}'} \tag{3.23}$$

We see that (3.22) may be written

$$\partial_t |P(s,t)\rangle = \widehat{W} |P(s,t)\rangle \tag{3.24}$$

and has the formal solution

$$|P(s,t)\rangle = e^{t\widehat{W}} |P_0\rangle \tag{3.25}$$

in terms of the initial state vector $|P_0\rangle = \sum_{\mathcal{C}} P_A(\mathcal{C}, s, 0)\,|\mathcal{C}\rangle$. Thus, the problem is fully specified by the *spectrum* of $\widehat{W}$. In particular, long-time behaviour is dictated by the largest eigenvalue λ_0:

$$|P(s,t)\rangle \sim e^{t\lambda_0}\,|R_0\rangle \tag{3.26}$$

with $|R_0\rangle$ the associated right eigenvector.[15] But from (3.18) and the decomposition (3.20), at long times the coefficients of $|P(s,t)\rangle$ behave as

$$Z_A(s,t) = \sum_{\mathcal{C}} P_A(\mathcal{C}, s, t) \sim e^{t\psi(s)} \tag{3.27}$$

Therefore the greatest eigenvalue is just $\psi(s)$.

The power for this formulation is that we can now make use of common operator methods from linear algebra. A most useful one is provided by the *Rayleigh–Ritz* theorem (Appendix D.1). This applies to Hermintian (here symmetric) operators, so it is firstly necessary to symmetrise $\widehat{W}$. Guided by the property of detailed balance (3.12), this is achieved with the similarity transform

$$W_{\mathcal{C}\mathcal{C}'} \to \widetilde{W}_{\mathcal{C}\mathcal{C}'} = P_{\mathrm{eq}}(\mathcal{C})^{-1/2}\,\widehat{W}_{\mathcal{C}\mathcal{C}'}\,P_{\mathrm{eq}}(\mathcal{C}')^{1/2} \tag{3.28}$$

resulting in (Appendix D.2)

$$\widetilde{W}_{\mathcal{C}\mathcal{C}'} = e^{-s}\left[W(\mathcal{C}\to\mathcal{C}')\,W(\mathcal{C}'\to\mathcal{C})\right]^{1/2} - r(\mathcal{C})\,\delta_{\mathcal{C}\mathcal{C}'} \tag{3.29}$$

The theorem then provides

$$\lambda_0 = \psi(s) = \max_{|V\rangle} \frac{\langle V|\widetilde{W}|V\rangle}{\langle V|V\rangle} \tag{3.30}$$

where the maximum is to be taken over all nonzero vectors excluding, in mind of irreducibility, the null configuration. With sensibly chosen $|V\rangle$ the quotient appearing here may be calculated explicitly, allowing one to place bounds on $\psi(s)$. We put this to use below.

3.3 Dynamical Phase Transitions

So far we have defined the SCGF or dynamical free energy per unit time $\psi(s)$ in the long-time limit for a finite system of size N. We now take $N \to \infty$ also and show that the dynamical free energy *density* $\psi(s)/N$ has a discontinuity in its *first* derivative at $s = 0$. In accord with the thermodynamic analogy, this is interpreted as a dynamical *first-order* phase transition.

The following proof is based on that set out by Garrahan et al. in their 2009 paper[16] [5]. This relies on properties of both the escape rates $r(\mathcal{C})$ and the equilibrium distribution P_{eq} known for the FA and East models. The same properties, and so the final result, hold for all KCMs of similar type. It may be helpful to refer to Figure 3.4 which summarises the proof.

[15] Equation (3.26) is corret to $O(e^{t\Delta})$ where Δ is the gap between λ_0 and the next largest eigenvalue λ_1 [2]. See [5, App. A.1] for a discussion of the eigensystem of $\widehat{W}$.

[16] The proof has been reorganised into what I consider a clearer order. In addition, a simple argument is given for the equilibrium value (3.33) and this quantity is calculated explicitly for the FA and East models.

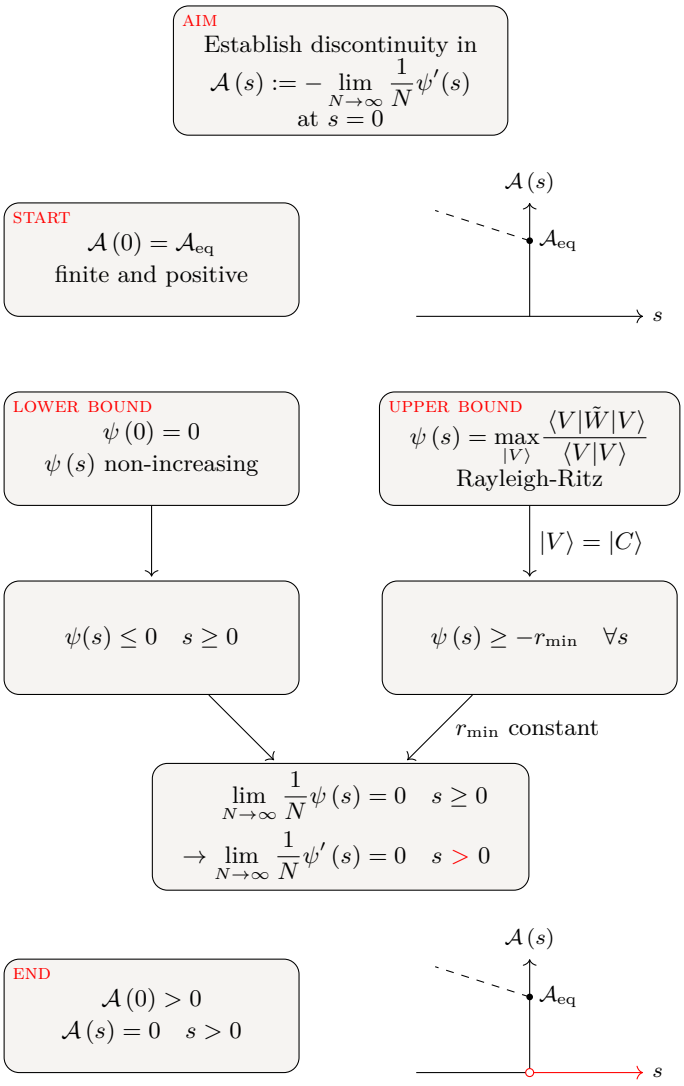

Figure 3.4: Outline of the proof of a dynamical first-order transition in kinetically constrained models.

3.3.1 Existence of a First-order Transition in KCMs

The quantity of interest is

$$\mathcal{A}(s) = -\lim_{N\to\infty} \frac{1}{N}\psi'(s) \tag{3.31}$$

We look to establish a discontinuity in $\mathcal{A}$ at $s = 0$. Recalling that the derivatives of $\psi(s)$ determine the moments of $\bar{a} = A/Nt$ (cf. (2.20)), $\mathcal{A}(s)$ has the interpretation of a *mean* rate of activity per site in the s-ensemble. In particular, the value at $s = 0$,

$$\mathcal{A}(0) = -\lim_{N\to\infty} \frac{1}{N}\psi'(0) = \lim_{N\to\infty}\lim_{t\to\infty} \langle A/t\rangle \tag{3.32}$$

features the steady-state we know is described by $P_{\rm eq}$ in (3.3). Hence $\mathcal{A}\,(0)$ is determined by the rate of transition from each configuration $\mathcal{C}$ weighted according to this distribution:

$$\mathcal{A}_{\rm eq} := \mathcal{A}\,(0) = \lim_{N\to\infty} \frac{1}{N}\sum_{\mathcal{C}} P_{\rm eq}\,(\mathcal{C})\, r\,(\mathcal{C}) \tag{3.33}$$

The simple form of $P_{\rm eq}$ and the local nature of the constraints in the models makes this limit straightforward to evaluate. Firstly, leaving a configuration $\mathcal{C} = \{n_j\}$ involves change at a *single* site, so the escape rate may be written

$$r\,(\mathcal{C}) = \sum_{i=1}^{N} W\,(\mathcal{C}\to\mathcal{C}_i') \tag{3.34}$$

where $\mathcal{C}_i'$ differs from $\mathcal{C}$ at the $i^{\rm th}$ site only. Then

$$\sum_{\mathcal{C}} P_{\rm eq}\,(\mathcal{C})\, r\,(\mathcal{C}) = \sum_{i=1}^{N}\sum_{n_1}\cdots\sum_{n_N}\prod_{j=1}^{N} \frac{e^{-\beta n_j}}{1+e^{-\beta}} W\,(\mathcal{C}\to\mathcal{C}_i') \tag{3.35}$$

where we used (3.3) and wrote the sum over configurations explicitly. The sum over i was also brought to the left, a permissible move since all sums are finite. Now, in the FA model the value $W\,(\mathcal{C}\to\mathcal{C}_i')$ depends on n_i and its neighbours only, so the contribution to (3.35) from n_j for $j \notin \{i-1, i, i+1\}$ is trivial:

$$\sum_{n_j=0}^{1} \frac{e^{-\beta n_j}}{1+e^{-\beta}} = 1 \tag{3.36}$$

What remains involves an average $\langle W\rangle_3$ of $W\,(\mathcal{C}\to\mathcal{C}_i')$ over three sites:

$$\sum_{\mathcal{C}} P_{\rm eq} r\,(\mathcal{C}) = \sum_{i=1}^{N} \underbrace{\frac{1}{Z^3}\sum_{n_{i-1}=0}^{1}\sum_{n_i=0}^{1}\sum_{n_{i+1}=0}^{1} e^{-\beta n_j} W\,(\mathcal{C}\to\mathcal{C}_i')}_{:=\langle W\rangle_3}, \qquad Z \equiv \frac{1}{1+e^{-\beta}} \tag{3.37}$$

This average does not depend on the site index i (translation-invariance), hence

$$\mathcal{A}_{\rm eq} = \lim_{N\to\infty}\frac{1}{N} N\,\langle W\rangle_3 = \langle W\rangle_3 > 0 \qquad \text{(FA)} \tag{3.38}$$

$n_{i-1}n_in_{i+1}$	Contribution ($\times Z^3$)
000, 010	0
100, 001	$e^{-\beta}c$
101	$e^{-2\beta}c$
110, 011	$e^{-2\beta}(1-c)$
111	$e^{-3\beta}(1-c)$

(a)

$n_{i-1}n_i$	Contribution ($\times Z^2$)
00, 01	0
10	$e^{-\beta}c$
11	$e^{-2\beta}(1-c)$

(b)

Table 1: Contribution to each three or two spin state to the averages (a) $\langle W\rangle_3$ and (b) $\langle W\rangle_2$ in which the i^{th} variable changes. The rates are determined to the spin-flip rules (3.5) and (3.7) for the FA and East models, respectively (for example, $100 \to 110$ at rate c in both models). Using the expression $c = e^{-\beta}/Z$ for the mean excitation density ($1 - c = 1/Z$),

$$\langle W\rangle_3 = \frac{2e^{-2\beta}\left(2+e^{-\beta}\right)}{\left(1+e^{-\beta}\right)^4} \quad \text{and} \quad \langle W\rangle_2 = \frac{2e^{-2\beta}}{\left(1+e^{-\beta}\right)^3}$$

For the East model, the situation is even simpler as the behaviour at i depends exclusively on the state at $i-1$, giving the corresponding average over two sites:

$$\mathcal{A}_{\text{eq}} = \langle W\rangle_2 > 0 \qquad \text{(East)} \tag{3.39}$$

The quantities $\langle W\rangle_3$, $\langle W\rangle_2$ are calculated explicitly in Table 1 and provide a first point on the graph of $\mathcal{A}(s)$ (Figure 3.4). Recalling that $\psi(s)$ is (strictly) convex, $\psi'(s)$ is non-decreasing and so $\mathcal{A}(s) \geq \mathcal{A}_{\text{eq}}$ for $s < 0$ too. We now turn to determine $\mathcal{A}(s)$ along the positive s axis by bounding $\psi(s)$ (and so $\psi'(s)$) there.

An upper bound follows from the basic property $\psi(0) = 0$ and the fact that, since the activity is non-negative, e^{-sA} and so $\psi(s)$ is non-increasing:

$$\psi(s) \leq 0 \quad s \geq 0 \tag{3.40}$$

To obtain a lower bound, apply the variational result[17] (3.30) with $|V\rangle = |C\rangle$ a single configuration:

$$\psi(s) = \max_{|V\rangle} \frac{\langle V|\widetilde{W}|V\rangle}{\langle V|V\rangle} \geq \max_{\mathcal{C}} \frac{\langle \mathcal{C}|\widetilde{W}|\mathcal{C}\rangle}{\langle \mathcal{C}|\mathcal{C}\rangle} = \max_{\mathcal{C}} \left[-r\left(\mathcal{C}\right)\right] \tag{3.41}$$

Or, noting $\max_{\mathcal{C}} \left[-r\left(\mathcal{C}\right)\right] \equiv -\min_{\mathcal{C}} \left[r\left(\mathcal{C}\right)\right]$,

$$\psi(s) \geq -\min_{\mathcal{C}} \left[r\left(\mathcal{C}\right)\right] \quad \forall s \tag{3.42}$$

Having excluded the case $n_i = 0\ \forall i$, the minimum escape rate in the FA and East models comes from any configuration containing a single excitation. In d dimensions the lone excitation has $2d$ neighbours, giving $r_{\min} = 2dc$ for the FA model and $r_{\min} = dc$ for the East model where facilitation occurs in one direction only. In either case, $r_{\min}$ is a finite constant *independent* of N so

$$\lim_{N\to\infty} \frac{1}{N}\psi\left(s\right) \geq \lim_{N\to\infty} \frac{1}{N} \min_{\mathcal{C}}\, r\left(\mathcal{C}\right) = 0 \tag{3.43}$$

[17] Alternatively, the lower bound can be derived using methods from optimal control theory; see [2, Sec. 4.2].

Combining (3.40) and (3.43),

$$\lim_{N\to\infty}\frac{1}{N}\psi(s)=0 \quad s\geq 0 \tag{3.44}$$

from which

$$\lim_{N\to\infty}\frac{1}{N}\psi'(s)=0 \quad s>0 \tag{3.45}$$

The loss of equality $s\geq 0 \to s>0$ from (3.44) to (3.45) is crucial: one cannot conclude, in general, that a differentiable sequence of functions that converge to the zero function on a closed interval has a derivative that converges to zero at the end points of that interval (consider $f_N(s):=(1-x)^N/N$ on $[0,1]$). Indeed, we have a counterexample since we have now shown

$$\mathcal{A}(s)=-\lim_{N\to\infty}\frac{1}{N}\psi'(s)=0 \quad s>0 \quad \text{and} \quad \mathcal{A}(0)>0 \tag{3.46}$$

That is, a discontinuity of $\mathcal{A}(s)$ at $s=0$. □

In the following section we discuss the nature of the transition associated with this discontinuity and its relevance for glass forming systems. A complete treatment of the phenomena is beyond the scope of this essay. As such we refer the reader to several key works on the topic [24, 42–45] that they will hopefully be well-equipped if not inspired to consult after our overview.

3.3.2 Dynamical Phase Coexistence

Phase transitions are synonymous with critical phenomena and, in the case of a first-order transition, *phase coexistence.* We now examine how coexistence in the space-time domain may offer an explanation of heterogeneous relaxation in glass forming liquids.

Firstly, a reminder of the conventional phenomena. Figure 3.5a depicts the phase diagram of the two-dimensional Ising model, a lattice of spins with ferromagnetic couplings and subject to a magnetic field H. In the thermodynamic limit $N\to\infty$, the average spin (magnetisation) m, a parameter that distinguishes different orderings or *phases* of the system, may change discontinuously as H is swept through 0. This is, of course, a statement of a singularity in first derivative of the bulk free energy density with respect to H (Figure 3.5b). Along the line of first-order transitions it is possible for the two different phases $m>0$, $m<0$ to coexist, with domains of each phase arranged so as to minimise the energy cost associated with any interface between them.

The analgous dynamical phase diagram is shown in Figure 3.5c. As in the Ising model, a field s drives the order parameter $\mathcal{A}$ through the transition and at vanishing field there is a coexistence of phases, in this case an active $\mathcal{A}(s)>0$ ($s<0$) and an inactive $\mathcal{A}(s)=0$ ($s>0$) one. This also reflects a discontinuity in the associated free energy density $\psi_N=\psi/N$ as $N\to\infty$ (Figure 3.5d). Note that ψ_N is analytic at each N; it is only in the limit that non-analyticity arises. This mirrors conventional thermodynamics, where true phase transitions occur in infinite systems only. Using the method of supporting lines from Section 2.1.4, we can construct the corresponding limit of the rate function for the activity, which is also non-analytic (Figure 3.6b).

The origin of dynamical heterogeneity has emerged: active and inactive phases coexist in our system corresponding to mobile and immobile (non-ergodic) phases of some putative glass former. Quite generally systems of discrete spins form distinct phases with sharp boundaries, so we might expect a dominant phase to surround well-defined 'droplets' of the other. Simulations of the models indeed reveal such 'bubbles' in space-time (Figure 3.7).

In order to be more precise about what will be observed in a simulation, we need to examine the steps we took in our large deviation analysis and their implications for the modelling of a

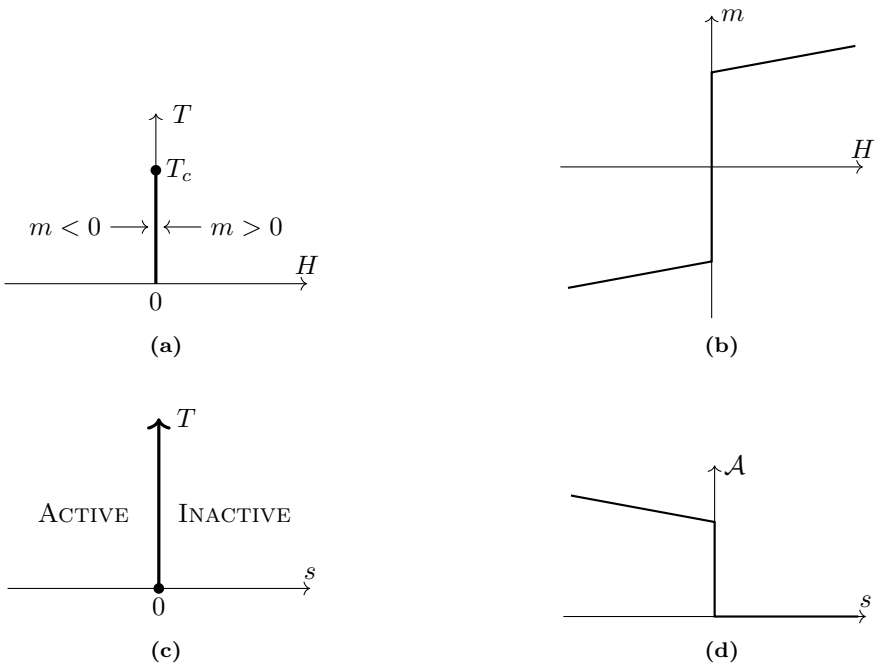

Figure 3.5: (a) Phase diagram for the 2D Ising model. Below T_c, changing H from positive to negative values results in (b) a discontinuous change in the magnetisation $m = -\lim_{N\to\infty} \frac{1}{N}\frac{\partial F}{\partial H}$ (F the free energy). (c) & (d) The analogous situation in trajectory space with a line of first-order dynamic transitions at $s = 0$.

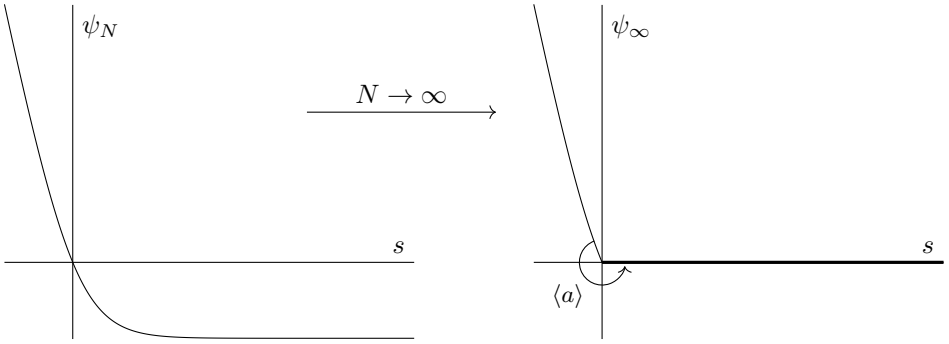

(a)

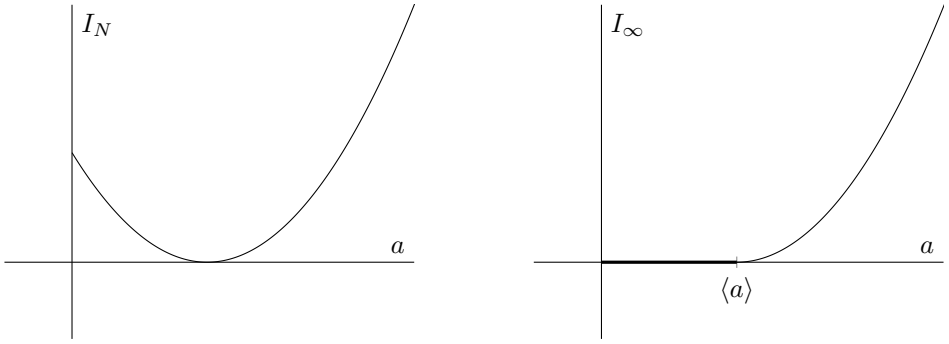

(b)

Figure 3.6: (a) Sketch of the free energy density $\psi_N := \psi/N$, a strictly convex function such that $\psi_N(0) = 0$, and its large system limit $\psi_\infty := \lim_{N\to\infty} \psi_N$. This form was verified numerically in [5, Fig. 4]. (b) Using the techniques set out in Section 2.1.4, we can sketch the associated sequence of scaled rate functions I_N (for $\bar{a}$) and their limit: The left and right derivatives of ψ_∞ at the origin are $-\langle a \rangle$ and 0, so the branch of ψ_∞ on $(-\infty, 0)$ is mapped to the branch on $(\langle a \rangle, \infty)$ of I_∞ and the non-differentiable point $(0, 0)$ to the interval $(0, \langle a \rangle)$ upon which I_∞ vanishes. This last interval is known as the phase coexistence region [9].

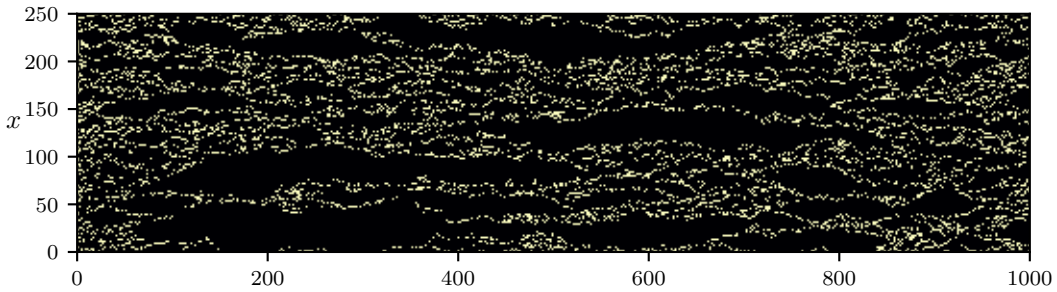

Figure 3.7: In a simulation of the FA model ($N = 250$), regions of inactive (dark) phase are surrounded by active (bright) phase. These regions have been called 'bubbles in space-time' [24, 46]. Note how the inactive domains are of greater extent in the t direction than in the x direction (interface parallel to the t-axis). Own work.

finite system. Recall that we are studying ensembles of trajectories, not one-time configurations. Thus given a d-dimensional lattice we have a $(d + 1)$-dimensional problem in space-time: N characterises the size of the system in each spatial direction and t the size in time. Initially, there was no particular bias for space or time. However, we took $t \to \infty$ at fixed N *before* $N \to \infty$, meaning $t/N \to \infty$ for our system. This is contrary to standard thermodynamic analysis where *aspect ratios* are normally held constant. The consequences of a diverging aspect ratio has been considered for conventional systems [47, 48] and more recently summarised in the context of space-time thermodynamics [2, Sec. 3].

When $t/N = O(1)$, one has the usual behaviour of thermodynamic phase coexistence associated with a bimodal probability distribution, such as that in Figure 3.8a where peaks at activity densities a_I and a_A characterise the inactive and active phases. That domains of these phases form with interfaces parallel to the t-axis in Figure 3.7 is indicative of a lower interfacial cost in this direction [45].

In contrast, when $t \gg N$ coexistence is realised by a *unimodal* probability distribution and interfaces *perpendicular* to the t-axis (Figure 3.8b). Thus as t is increased relative to N we expect to see a crossover from a situation where successive domains are arranged along x to one where they are arranged along[18] t (see Figure 3.8 insets). Both behaviours contrast with that for a system of independent spins, where there is no coexistence and less active trajectories are associated with a uniform reduction of activity density across the entire system.

What reason do we have to believe that this description is applicable to *real* glass forming liquids? Shortly after publication of the paper we have been focused on ([5], 2009), Hedges et al. presented numerical evidence for a dynamical first-order in atomistic models of supercooled liquids [43]. Using successive mean-square displacements of particles as a measure of activity, the group identified active (ergodic) and inactive (non-ergodic) phases in their model, with macroscopic volumes of these phases found to coexist (Figure 3.9). The significance of this result

[18]For further details, refer to [45] where phase coexistence was considered for the FA model, including a simple interface model.

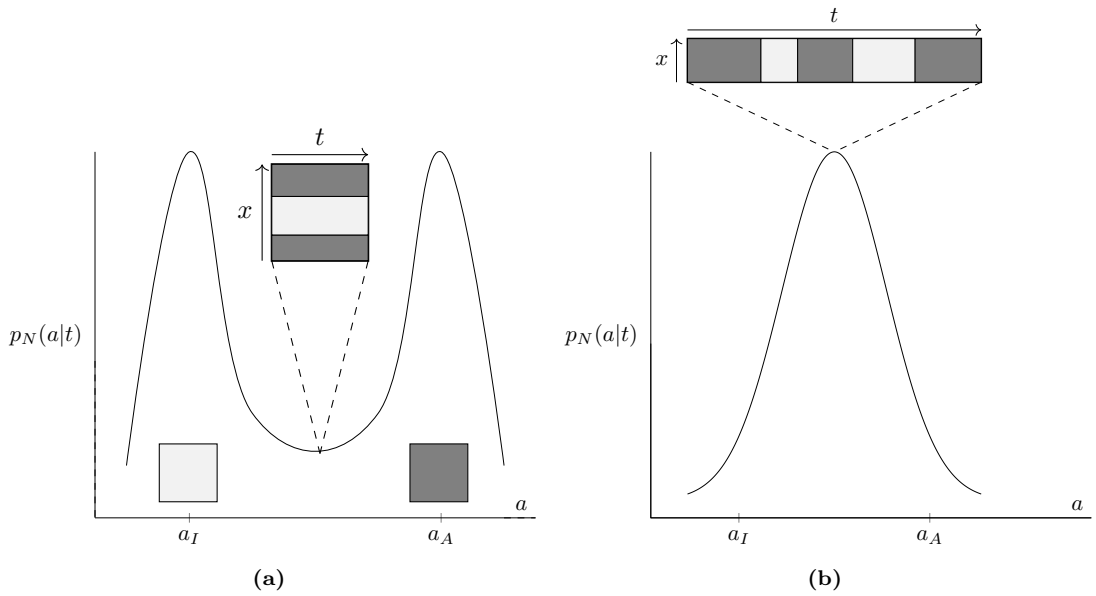

Figure 3.8: Aspect ratio and phase coexistence. (a) For $t/N = O(1)$, the probability density is bimodal, with a_I, a_A characterising the activity density of the inactive (light) and active (dark) phases (note $a_I > 0$; the configuration $n_i = 0\ \forall i$ is forbidden). Inset: At coexistence, domains of these phases are arranged parallel to the time axis. (b) When $t \gg N$, the distribution is instead unimodal and large domains of each phase are arranged along the time axis. After [45, Fig. 4].

is in the move from highly schematic models (KCMs) to more realistic ones.[19]

Another approach to this end is to *soften* the constraints of KCMs, allowing them to be violated with some small probability. The consequence for the phase diagram [55] is that the line of first-order transitions is bent from the T axis towards positive s and terminates at a finite temperature critical point (Figure 3.10). That the transition occurs at $s > 0$ in more realistic models, and by extension real glass formers, is supported by the observation of Hedges et al. that this was the case for their atomistic model [43].

To summarise, dynamic heterogeneity in KCMs is the phase coexistence phenomena of a first-order dynamical phase transition, and studies of atomistic models suggest that this might be the case for real glass forming liquids too. This could be indicative of a more general connection between glassy behaviour and dynamical phase transitions [5].

That draws to a close our investigation of glass formers and classical slow dynamics. We have, in kinetically constrained models, realised the principal features of glassy slowdown: stretched exponential response, super-Arrhenius timescales and dynamic heterogeneity. Next we look as to what insight the models might bring to studies of quantum systems.

4 Slow Quantum Relaxation

In this section we learn that the mechanisms responsible for classical glassy behaviour can produce slow relaxation and non-ergodic behaviour in quantum systems too. This has significance in the

[19] Hedges et al. considered a Kob-Anderson (KA) binary mixture [49] which is frequently used to model viscous fluids and glasses [50] and has now been well studied in relation to dynamical phase transitions [51–54].

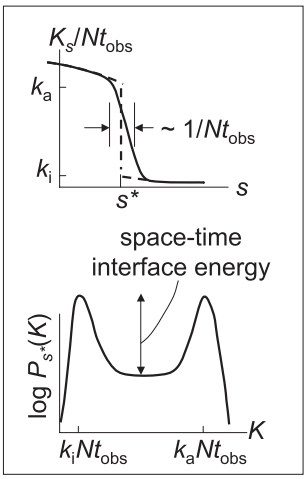

Figure 3.9: Schematic presented by Hedges et al. for the dynamical first-order phase transition in an atomistic model [43]. Here K denotes the activity and k_a, k_i values of activity density characterising the active and inactive phase. **Top.** It is only possible to simulate a finite system, so a crossover is observed instead of a sharp transition; the width of this crossover vanishes with $t_{\text{obs}}N \to \infty$. **Bottom.** (Negative) Logarithm of the dynamical activity distribution. The minimum of this plot corresponds to the maximum of that in Figure 3.8b. Reprinted with permission from AAAS.

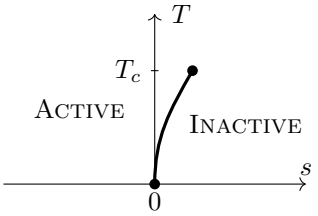

Figure 3.10: More realistic phase diagram obtained from softening the constraints of the FA model [55]. The scaling behaviour in the vicinity of the new finite-temperature critical point T_c is analogous to that near a liquid-vapour transition.

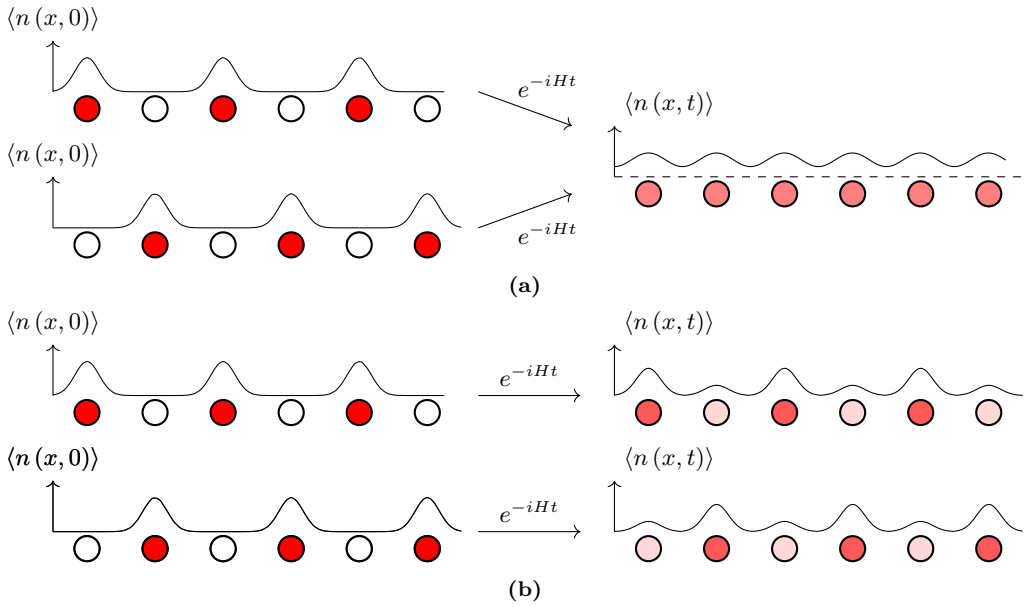

Figure 4.1: Quantum particles on a lattice. (a) In a thermalising system, memory of initial conditions – here particle densities – is erased as the system relaxes to a thermodynamic state in which all sites are equally populated. (b) In the case of localisation, thermal equilibrium is never achieved and information from the initial state persists in the system, even at long times (after equilibration). After [56].

highly active research topic of many-body localization (MBL). We examine the results of the 2015 article [6] by van Horssen et al. in which a quantum East model was studied in this context. It is firstly necessary to discuss the nature of *quantum ergodicity.*

4.1 Ergodicity in Closed Quantum Systems

4.1.1 Equilibration and Thermalisation

Recall that ergodicity concerns the long-time behaviour of a system: do time-averages converge to the ensemble average of a unique steady-state? We consider quantum systems that are *closed* (isolated from their environment) for which this steady-state should be a thermal one, predicted by the microcanonical ensemble. There are then two aspects of the question to address.

The first is whether the system *equilibrates,* meaning that the long-time expectation values of observables become stationary and close to their time-averages. The second, *thermalisation,* is whether this stationary behaviour is unique, i.e. independent of initial conditions, and well described by a thermal state.[20] Note that the first does not necessarily imply the second – different starting configurations can lead to different stationary states. Quantum ergodicity, then, requires *thermal equilibration.* These ideas are illustrated in Figure 4.1.

A large number of closed quantum systems are observed to thermalise [16]. Those that do not are said to *localise* and have late-time states that cannot be described by equilibrium statistical mechanics [59]. While examples of non-interacting localised systems have long been

[20] A thermal state $\rho_{\text{th}} = e^{-\beta H}/Z$ is determined by the (conserved) energy of the system so, more accurately, the only memory retained is that of the initial energy. For an introduction thermalisation in closed quantum systems, see the lecture by J. Garrahan [16, Sec. 3] or recent reviews [56–58] of the subject.

known, there has recently been great interest in strongly interacting many-body systems that fail to thermalise, the phenomena of many-body localisation (MBL). Common to these systems appears to be the presence of static disorder (for example, a spin-chain with fields h_i at each site drawn from a random distribution [60]). On the contrary, the occurrence of MBL in a translation-invariant system has never been verified [61]. We arrive at the motivation for the paper [6] under consideration: the search for a MBL in a finite translation-invariant system.

4.1.2 Signatures of MBL

The emergence of MBL is akin to a quantum glass transition in that ergodicity is lost and equilibrium statistical mechanics ceases to apply [62].[21] Just like the classical phenomena, there are distinct dynamical features to identify: evolution to the final state is characterised by slow, logarithmic changes; namely in the spreading of excitations and the growth of entanglement entropy (Appendix E.1) [60]. From these changes relaxation timescales can be calculated which are observed to diverge with increasing *system size* [6].

For a candidate MBL phase the key question is often whether relaxation timescales are truly divergent or remain finite but numerically inaccessible. This is another parallel with the glass transition problem where, as we have seen, it is contended whether τ diverges at a finite temperature or not. If timescales are only numerically inaccessible, the localised behaviour is transient and ergodicity is expected to be restored at very long times – a situation referred to as *quasi*-MBL.

4.2 Quantum East Model

4.2.1 A Rokhsar-Kivelson Point

The model considered by van Horssen et al. [6] comprised a chain of spin-1/2 degrees of freedom with Hamiltonian

$$H = \frac{1}{2}\sum_{i=1}^{N} n_i - e^{-s}\sigma_i^x n_{i-1} \tag{4.1}$$

where $n_i := (1+\sigma_i^z)/2$ projects onto the up state $|\uparrow\rangle$ of the local z-basis and σ_i^α is the α-Pauli operator at site i. Periodic boundary conditions are prescribed so that the system is manifestly translation-invariant.

This model is closely related to the classical East model from Section 3.2.1. To make the connection, firstly take $s = 0$ and compare the structure of Schrödinger equation

$$i\partial_t |\psi\rangle = H|\psi\rangle = \frac{1}{2}\sum_{i=1}^{N}(n_i - \sigma_i^x n_{i-1})|\psi\rangle \tag{4.2}$$

with that of the master equation (cf. (3.10))

$$\partial_t P(\mathcal{C},t) = -r(\mathcal{C})P(\mathcal{C},t) + \sum_{\mathcal{C}'} W(\mathcal{C}'\to\mathcal{C})P(\mathcal{C}',t) \tag{4.3}$$

which we recall governs the dynamics of the classical model with rates parametrised by the excitation density c. In the high temperature limit, $c = 1-c = 1/2$ and the escape rate $r(\mathcal{C})$ is

[21] Naturally, the characteristic of the glass transition we might hope to realise in defining a *quantum* East model is that is occurs in translation-invariant systems (liquids). The connection between the classical and quantum models is detailed below.

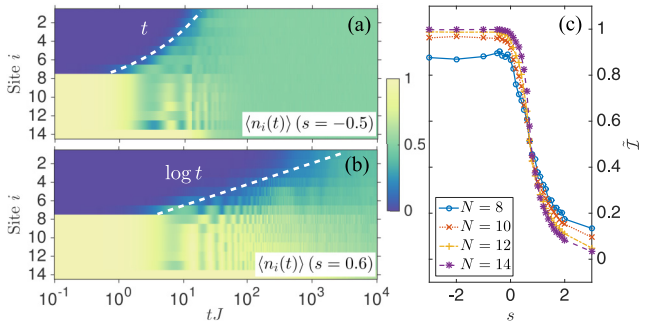

Figure 4.2: Expectation value of the site densities $\langle n_i(t)\rangle$ from the starting configuration $|\downarrow \ldots \downarrow\uparrow \ldots \uparrow\rangle$ for the proposed (a) thermal and (b) athermal regimes. (c) Long-time value of the inverse participation ratio, averaged over all half-filled initial states at a certain s, N. Its value decays as $O\left(N^{-1}\right)$ for $s > 0$ [6], indicating localisation (see Appendix E.2). Reprinted figure with permission from [6]. Copyright 2020 American Physical Society.

simply a sum over all active sites (up spins) $n_i = 1$ multiplied by $1/2$ since any active site can facilitate the excitation or relaxation of its right (east) neighbour. Hence a direct correspondence with the first term of H. Similarly, the transition rate from a configuration differing at site i is either $1/2$, when $n_{i-1} = 1$, or 0, when $n_{i-1} = 0$. This is captured by the second term of H, since the x-Pauli matrix σ_i^x acts to produce a state vector with spin i inverted ($\sigma_i^x |\uparrow\rangle = |\downarrow\rangle$, $\sigma_i^x |\downarrow\rangle = |\uparrow\rangle$) and the operator n_{i-1} ensures that it does so only when the spin at $i-1$ is excited.

In this way H is, up to a sign, equivalent to the master operator of the classical model at infinite temperature, albeit generating imaginary time dynamics. This correspondence is an example of one found to occur quite generally[22] between a classical stochastic operator and a quantum Hamiltonian in which a parameter, typically one controlling the ratio of kinetic and potential terms, is tuned to a particular value (here $s = 0$) known as a *Rokhsar-Kivelson* point [64, 65]. Of course, we have also worked with $s \neq 0$ (the s-ensemble) in which case H becomes the analogous 'tilted' operator [6].

On account of the classical result then, we might expect H to be associated with regimes of both fast and slow relaxation, and this is exactly what is found. Figure 4.2 illustrates the time evolution of site densities $\langle n_i(t)\rangle$ from the half-filled initial state $|\downarrow \ldots \downarrow\uparrow \ldots \uparrow\rangle$ [6]. For $s < 0$, excitations spread linearly and relaxation is fast, whereas for $s > 0$ a logarithmic spreading of excitations indicates slow relaxation and a lack of thermalisation. Supporting this observation is the plot of the inverse participation ratio, a quantity that provides a direct measure of localisation (Appendix E.2) and should decay to zero for a localised state. Thus we have evidence that $s < 0$ and $s > 0$ describe thermal and nonthermal regimes, respectively, with $s \approx 0$ delimiting a MBL transition. Following the signatures described above, to be more certain we should examine initial state dependence and the growth of entanglement entropy in the proposed athermal regime.

4.2.2 Initial Conditions and Entropy Growth

Since it is groups of down spins that frustrate relaxation in the East model, a sensible way of grouping possible initial configurations of the same energy is according to the *maximum* number

[22] Remarkably, for any classical model with a finite number of configurations and dynamics satisfying detailed balance it is possible to construct a quantum Hamiltonian such that the ground state wavefunction coincides with the classical equilibrium distribution [63]. The connection is deep and interesting [64].

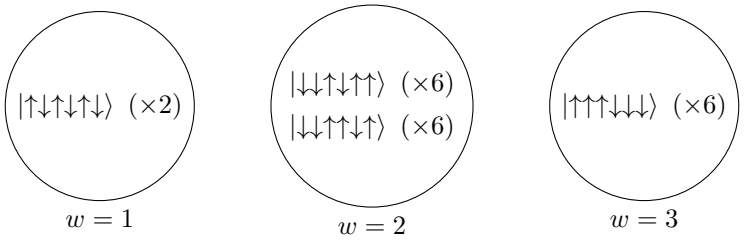

Figure 4.3: Possible starting configurations for $N = 6$ spins sorted according the maximum number of consecutive down spins, w. Multipliers indicate cyclic permutations which are indistinguishable on account of the periodic boundary conditions (translation-invariance).

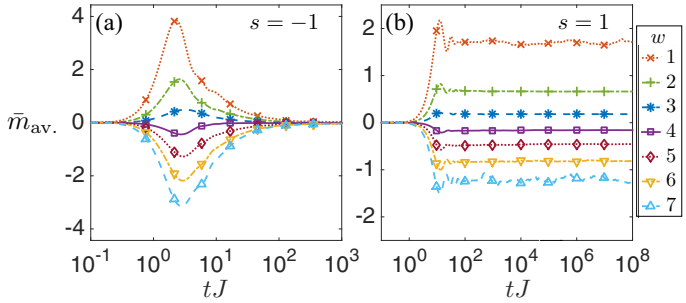

Figure 4.4: Time-averaged magnetisation averaged over realisations with the same number of maximum consecutive down spins w ($N = 14$). J is an energy scale that was set to 1. (a) For $s < 0$, the variance at intermediary times (expected since different initial states evolve differently) quickly decays. (b) For $s > 0$, different initial states result in different long-time values of $\bar{m}_{\text{av.}}$. Reprinted figure (adjusted) with permission from [6]. Copyright 2020 American Physical Society.

of consecutive down spins w (Figure 4.3). As for a dynamical observable to follow, an obvious one is the time-averaged total spin or magnetisation

$$\bar{m}(t) = \frac{1}{t}\int_0^t m(\tau)\, d\tau \quad \text{where} \quad m(\tau) := \langle\psi(t)|\sum_i \sigma_i^z|\psi(t)\rangle \tag{4.4}$$

Figure 4.4 shows the evolution of this quantity starting from an initial state randomly selected from the half-filled sector and averaged over half-filled states of equal w, for different values of w. For $s < 0$, $\bar{m}_{\text{av.}} \to 0$, the thermodynamic expectation value. This occurs relatively quickly and regardless of the value of w. In contrast, behaviour for $s > 0$ is distinctly non-thermal, with the final value of $\bar{m}$ strongly dependent on the starting configuration.

Tracking the growth of entanglement entropy $S(t)$ requires a little more thought. As explained in Appendix E.1, the system should be partitioned; we consider splitting the chain into two equal parts, with cuts after site i and $i + N/2$ say. In order to respect translation-invariance, any measurement of $S(t)$ should be averaged over all possible choices of cut location [6]. The results are collated in Figure 4.5: $\bar{S}(t)$ grows exponentially in the thermal regime and logarithmically in the athermal regime, corroborating our earlier observations. Moreover, the long-time value of $\bar{S}$ in the second case appears to depend on the initial configuration (w). From these entropy plots van Horssen et al. calculated a relaxation time from the time taken for $\bar{S}(t)$ to fall within some small window of its final value. This was found to grow exponentially with N at $s > 0$, at

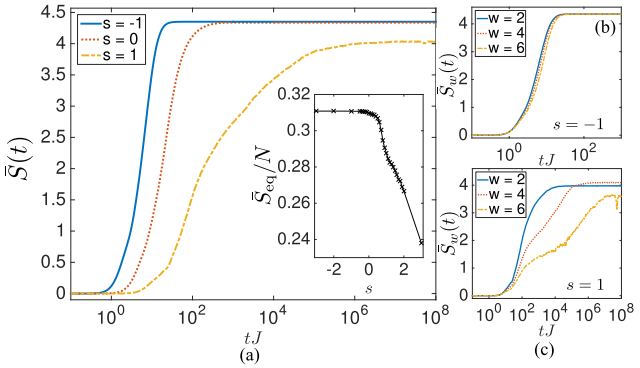

Figure 4.5: (a) Entanglement entropy $\bar{S}(t)$ averaged over equal bipartitions of the spin-chain. In the thermal regime ($s < 0$) growth is exponential to a final equilibrium value $\bar{S}_{\rm eq}$ which is independent of both s (see inset) and (b) w. In contrast, for $s > 0$ growth is logarithmic and $\bar{S}_{\rm eq}$ varies with s and (c) w. Reprinted figure with permission from [6]. Copyright 2020 American Physical Society.

least for the range of values ($N \leq 14$) they were able to consider [6].

4.2.3 Conclusions

What have we learnt from the above results? Foremost, that that the same type of local constraints that give rise to classical glassy behaviour can produce slow relaxation in quantum systems too. As for localisation, while we have certainly observed the leading characteristics of MBL, *proving* that this is the case is another matter. It could be that, at even longer times, beyond those feasible to simulate, ergodicity is restored.

Indeed, to to this date it remains unclear whether translation-invariant systems can exhibit true MBL, although there are many candidates: in addition to the East model, the FA model has also been used as a starting point [66], with other possibilities in the form of Hubbard-like [67] and hard-core bosonic models [68].

5 Outlook

In this essay we have explored examples of slow dynamics in relation to (i) the classical glass transition problem and (ii) quantum many-body localisation. The main ideas were how kinetic constraints can lead to slow dynamics, the usefulness of time-averaged quantities and their large deviations in assessing these dynamics, and ergodicity loss.

There is of course, much more to be said. For the glass transition problem, connecting the dynamical description we have examined to the thermodynamics of real super-cooled liquids such as their heat capacity (Figure 5.1a), and more generally structural aspects of the transition, presents a challenging research direction [53, 69, 70]. Another connection to be developed is between glass formation and the occurrence of *jamming* in colloids and granular packings (Figure 5.1b). This is an athermal phenomenon yet also associated with slow, heterogeneous dynamics [71, 72].

There is a great deal more to investigate in the *dynamics* of glass forming systems too. We have been concerned with primary or α-relaxation timescales of structural relaxation. There are

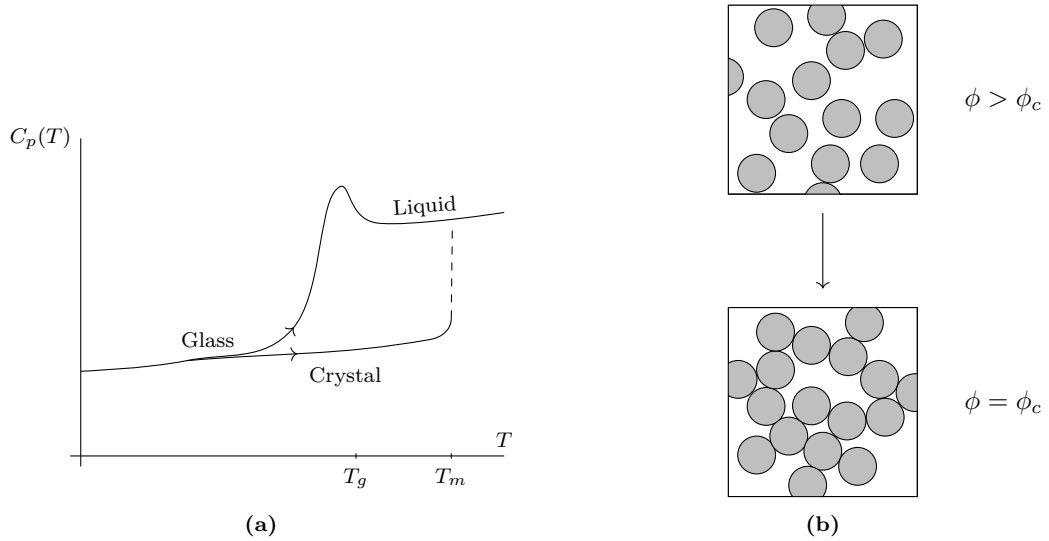

Figure 5.1: Thermodynamic response and jamming. (a) Schematic for the specific heat of crystalline, glass and liquid forms of a typical covalent glass former (after [4]). A sharp but continuous rise marks the glass-liquid transition. (b) Jamming describes how rigidity may develop in a system as the packing fraction ϕ of particles is decreased: at some critical value ϕ_c there are sufficient contacts between particles for the system to become load bearing (after [3]).

however a host of secondary β-relaxation processes[23] which occur over much shorter timescales τ_β. Less is known about these processes in glass-formers and an important question is what bearing they have on α-relaxation and so the transition [28, 73–75].

With kinetically constrained models, there is scope to uncover novel behaviour through the adjustment of dynamical rules and parameters. We have already seen how softening the constraints of the FA effects the dynamical phase diagram (Figure 3.10). Recently, a similar softening was considered for an East model with the outcome of accelerated relaxation and suppressed heterogeneity [76].

The study of slow dynamics in quantum systems is a vast and rapidly evolving field of which have touched on only one, albeit significant, topic. Another of particular relevance to this essay is the study of jump trajectories in *open* Markovian quantum systems [77–79]. Here too large deviation methods can be applied [80] to understand dynamical phases, complete with phase transitions and glassy behaviour [81–83].

Looking to the bigger picture, slow dynamics in interacting systems – be it relaxation or transport – is a fundamental unsolved problem that extends into many domains of science and engineering [28]. Even modest advancement of a coherent theory of these processes would undoubtedly have far-reaching consequences.

Acknowledgements

I wish to thank the setter of the essay title, Dr Rob Jack, whose correspondence has provided much guidance and made the experience of writing this essay a particularly rewarding and enjoyable one.

[23] Loosely, these involve the vibration motion of particles in the 'cages' formed by their neighbours [73]. See [33] for a review.

A Mathematical Results

A.1 $P(S_N)$ Large N Approximation

Stirling's formula is

$$f(N) = \sqrt{2\pi} N^{N+1/2} e^{-N} \tag{A.1}$$

It is asymptotically equivalent to $N!$, written $f(N) \sim N!$ and meaning

$$\frac{f(N)}{N!} \to 1 \text{ as } N \to \infty \tag{A.2}$$

$f(N)$ is also a good approximation for $N!$ in the ordinary sense, even for quite small N (at $N = 10$ the relative error is .83%). With reference to (2.2) we have, for large N, $k = rN$ and $N - k$ (i.e. not too close to either tail of the distribution),

$$P(S_N = r) \sim \frac{1}{2^N} \frac{f(N)}{f(k) f(N-k)} \tag{A.3}$$

$$= \frac{1}{\sqrt{2\pi}} \frac{1}{2^N} \frac{N^{N+1/2}}{k^{k+1/2} (N-k)^{N-k+1/2}} \tag{A.4}$$

$$= \frac{1}{\sqrt{2\pi}} \sqrt{\frac{N}{k(N-k)}} \frac{1}{2^N} \frac{N^N}{k^k (N-k)^{N-k}} \tag{A.5}$$

$$= \frac{1}{\sqrt{2\pi N r(1-r)}} g(k(r)) \tag{A.6}$$

where

$$g(k(r)) = \frac{1}{2^N} \frac{N^N}{k^k (N-k)^{N-k}} \tag{A.7}$$

$$\to \ln g(r) = -N \ln 2 + N \ln N - k \ln k - (N-k) \ln (N-k) \tag{A.8}$$

$$= -N [\ln 2 - \ln N + \ln (N-k) + r \ln k - r \ln N + r \ln N - r \ln (N-k)] \tag{A.9}$$

$$= -N I(r) \tag{A.10}$$

with

$$I(r) = \ln 2 + r \ln r + (1-r) \ln (1-r) \tag{A.11}$$

A.2 Convexity of the SCGF

If p and q are positive real numbers such that $1/p + 1/q = 1$ and X is a measure space with measure μ, Hölder's inequality for two non-negative measurable functions f and g on X is [84]

$$\int_X f g d\mu \leq \left\{ \int_X f^p d\mu \right\}^{1/p} \left\{ \int_X g^q d\mu \right\}^{1/q} \tag{A.12}$$

When the measure space X is a probability space, for example of the random variable $\bar{b}$, this is a statement of expectation values,[24]

$$\langle fg \rangle \leq \langle f^p \rangle^{1/p} \langle g^q \rangle^{1/q} \tag{A.13}$$

[24] A clear introduction to measure and probability is given by Capinski & Kopp [85].

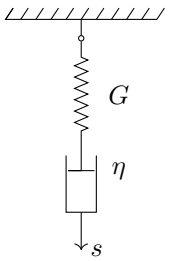

Figure B.1: The Maxwell model. A spring ($s = Ge_G$) conveys an elastic response and a dashpot ($s = \eta \dot{e}_\eta$) a viscous one.

To demonstrate that $\psi(s) = \lim_{t\to\infty} \frac{1}{t} \ln\langle e^{-st\bar{b}} \rangle$ is convex, let s_1, s_2 be arbitrary real numbers in the domain of ψ and $\alpha \in (0, 1)$. Define the positive measurable functions (parametrised by t)

$$f_t(\bar{b}) = e^{-\alpha s_1 t\bar{b}} \quad \text{and} \quad g_t(\bar{b}) = e^{-(1-\alpha)s_2 t\bar{b}} \tag{A.14}$$

Setting $p = 1/\alpha$, $q = 1/(1-\alpha)$ in (A.13),

$$\left\langle e^{-t\bar{b}(\alpha s_1 + (1-\alpha)s_2)} \right\rangle \leq \left\langle e^{-s_1 t\bar{b}} \right\rangle^{\alpha} \left\langle e^{-s_2 t\bar{b}} \right\rangle^{1-\alpha} \tag{A.15}$$

$$\to \frac{1}{t} \ln \left\langle e^{-t\bar{b}(\alpha s_1 + (1-\alpha)s_2)} \right\rangle \leq \frac{\alpha}{t} \ln \left\langle e^{-\alpha s_1 t\bar{b}} \right\rangle \frac{(1-\alpha)}{t} \ln \left\langle e^{-\alpha s_2 t\bar{b}} \right\rangle \tag{A.16}$$

since the logarithm is a non-decreasing function. Hence

$$\psi(\alpha s_1 + (1-\alpha)s_2) \leq \alpha\psi(s_1) + (1-\alpha)\,\psi(s_2) \tag{A.17}$$

B Modelling Relaxation

B.1 The Maxwell Model and Viscosity

We discuss a simple model of shear stress relaxation in order to gain an appreciation for how relaxation timescales characterise behaviour in a system disturbed from equilibrium.

The response of a material to mechanical stress can be broken down into two parts: an elastic part, modelled by a spring of elastic modulus G, and a viscous part, modelled by a dashpot of viscosity η. These components are defined by the stress-strain (s-e) relations

$$s = Ge_G \quad \text{and} \quad s = \eta \dot{e}_\eta \tag{B.1}$$

The Maxwell model consists of these two components in series (Figure B.1) [86]. Thus, it models a material that exhibits both elastic *and* viscous behaviour, or *viscoelasticity.* The applied stress is the same in both elements whilst the strains add hence

$$e_M = e_G + e_\eta \tag{B.2}$$

$$\to \dot{e}_M = \frac{\dot{s}}{G} + \frac{s}{\eta} \tag{B.3}$$

or

$$\dot{s} = G\dot{e}_M - \frac{G}{\eta}s \tag{B.4}$$

In experiment it is normally the case that a strain $e_M(0)$ is suddenly applied and then held constant. Under these conditions, (B.4) has solution[25]

$$s(t) = Ge_M(0)e^{-tG/\eta} = s(0)e^{-t/\tau_s} \tag{B.6}$$

which is of exponential form with stress relaxation time $\tau_s = \eta/G$.

While a single spring-dashpot is too simplistic to describe a real glass former, an array of n of these devices in parallel (different stresses, same strain) may be used for this purpose. For this *generalised Maxwell model* the solution to the considered stress relaxation experiment is no more than the sum of the solutions for each device [87]:

$$s(t) = Ge(0)\sum_{i=1}^{n} w_i e^{-t/\tau_i} \qquad \tau_i = \frac{G_i}{\eta_i} \tag{B.7}$$

where w_i are weighting factors. That this solution is appropriate reflects the fact that any stretched exponential function $e^{-(t/\tau)^b}$ may be written as a sum of linear exponentials [28]. Hence the non-exponential time dependence observed in glass formers may be viewed as arising from a superposition of exponential relaxation processes (the overall relaxation timescale a weighted average $\sum_i w_t\tau_i/n$).

For complete treament of viscoelasticity and mechanical relaxation, see the enduring collection edited by Uhlmann and Kreidl [87]. A more recent description of the Maxwell model and viscoelastic responses in glassy materials is given by Bourhisi [88]. The subject of relaxation processes in glass formers is a huge one of which we have presented a simplified view only. For those interested to find out more, the millennial review by Angell et al. [29] is comprehensive and provides a good basis for reading more recent studies in the field.

B.2 Overlap Function and Dynamic Susceptibility

Characterising fluctuations about averaged dynamical behaviour is important in the understanding of structural relaxations in glasses. These fluctuations are captured by time dependent distributions of particle displacements [89]. A quantity readily computed in numerical simulations for this purpose is the overlap function (or two-point density correlator) $\langle Q(t)\rangle$ [73], calculated as the ensemble average of

$$Q(t) = \frac{1}{N}\sum_{i=1}^{N} w\left(|\boldsymbol{r}_i(t) - \boldsymbol{r}_i(0)|\right) \tag{B.8}$$

where $\boldsymbol{r}_i(t)$ is the position of the i^{th} particle at a time t and $w(r)$ is a window function such that $w(r) = 1$ for $r < a_0$ and $w(r) = 0$ otherwise. Hence $Q(t)$ is a measure of the overlap of the system at t with its initial configuration, coarse grained according to a_0 (the precise value of

[25] This is determined by taking Laplace transforms: the applied strain conveys an impulse $\dot{e}_M = e_M(0)\delta(t)$ so, denoting the transform of s by $\hat{s} = \hat{s}(u)$ and using $s(0) = 0$,

$$u\hat{s} = Ge_M(0) - \frac{G}{\eta}\hat{s} \to \hat{s} = \frac{Ge_M(0)}{u + G/\eta} \to s = Ge_M(0)e^{-tG/\eta} \tag{B.5}$$

this parameter is qualitatively unimportant [90], but is typically of the order of a single particle diameter [73]).

The long time decay of $\langle Q(t)\rangle$ follows the stretched exponential familiar for glass formers [73]:

$$\langle Q(t)\rangle = e^{-(t/\tau_\alpha)^b} \qquad 0 < \beta < 1 \tag{B.9}$$

where τ_α defines the structural relaxation timescale of the system.

The dynamic susceptibility is then defined by the fluctuations of $Q(t)$ itself [90]:

$$\chi_4(t) = N\left[\left\langle Q(t)^2\right\rangle - \langle Q(t)\rangle^2\right] \tag{B.10}$$

This encodes dynamic correlations in the system and as such is important in the characterisation of dynamic heterogeneity (Section 2.2.3) [3]. Its maximum χ_4^M occurs at a time comparable to τ_α and provides a dynamical length scale which grows as the glass transition is approached [90].

C Simulating KCMs

C.1 Exponential Waiting Times

Continuous-time Markov dynamics are straightforward to realise with a computer program. Our KCMs present a particular simple case, due to the small number of possible transition rates (c, $1-c$ or c). The key observation is that these rates are *constants,* meaning that the time between transitions follows the exponential distribution.[26]

Consider first the system of independent spins in one dimension. Any spin that is initially down attempts to flip up at a constant rate c and so the waiting time τ for this event obeys

$$P_\downarrow(\tau = t) = ce^{-ct} \tag{C.2}$$

Similarly, each up spin attempts to flip down at a constant rate $1-c$ and so is attributed the exponential waiting time

$$P_\uparrow(\tau = t) = (1-c)e^{-(1-c)t} \tag{C.3}$$

In this way the system is a collection of *exponential timers,* each working independently and at a rate dependent on the state of the associated spin. To simulate evolution, it suffices to take successive samples from distributions (C.2) and (C.3) to obtain waiting times $\tau_1, \tau_2, \ldots$ for each spin until the sum $\tau_1 + \tau_2 + \ldots$ exceeds the intended simulation time t_f. One can imagine waiting for a timer with rate $\lambda \in \{c, 1-c\}$ to go off, resetting it with rate $1-\lambda$ and then repeating these two steps until $t = t_f$.

Having recorded these data, an image may be generated from the state of each spin at regularly spaced times $t_0, t_1, \ldots, t_f$ by placing at (t_n, i) a bright pixel if the spin at site i is up at t_n and a dark pixel if it is down (Figure C.1b).

[26] The waiting time can be calculated as the time for the first event in a Poisson process with rate $\lambda \in \{c, 1-c\}$; the probability of having to wait at least $T_1 > t$ for the event is equal to the probability of having recorded no ($n = 0$) events at t:

$$P(T_1 > t) = \frac{(\lambda t)^n}{n!}e^{-\lambda t}\bigg|_{n=0} = e^{-\lambda t} \tag{C.1}$$

which is the tail of the exponential distribution. The role of the exponential distribution in Poisson processes and continuous-time Markov chains is set out clearly in the textbook by Grimmett and Stirzaker [91].

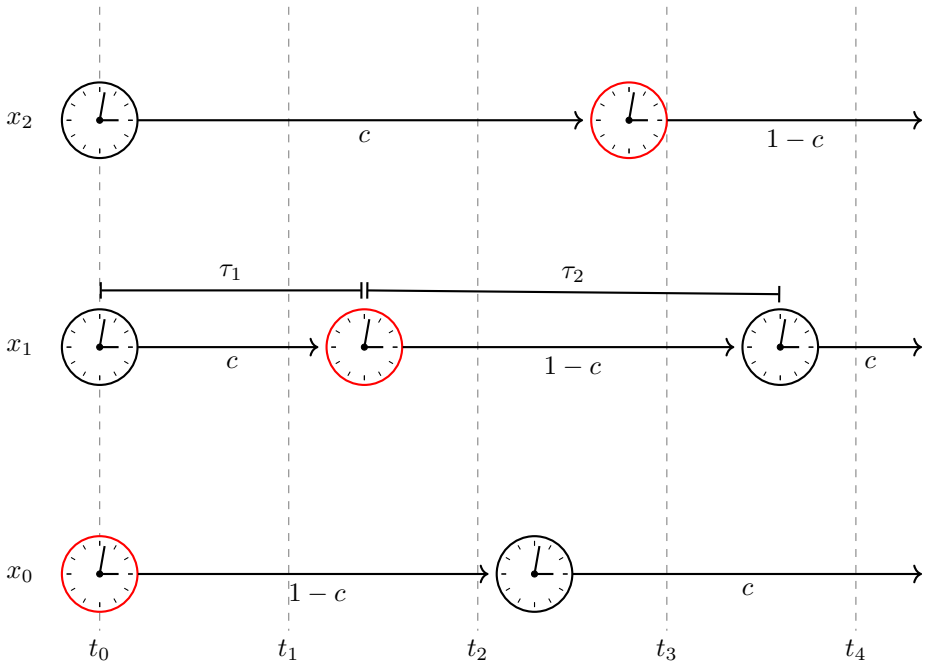

(a)

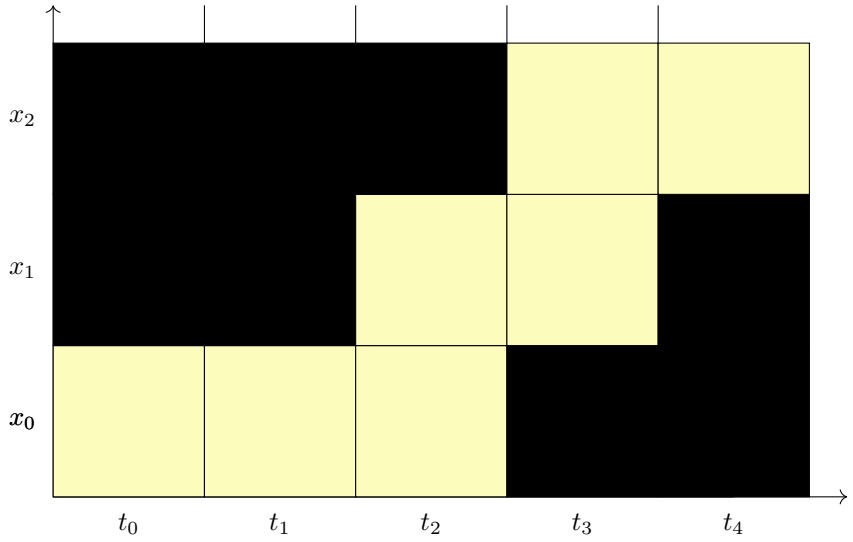

(b)

Figure C.1: Independent spins. (a) An exponential timer with rate c (black outline) models a down spin while an exponential timer with rate $1-c$ (red outline) models an up. The transition times $\tau_1, \tau_2, \ldots$ for the spin at x_1 are drawn from distributions (C.2) & (C.3). (b) The state of each site at times $t_0, t_1, \ldots$ is used to generate an image: a bright pixel represents an active site (red timer) and a dark pixel an inactive one (black timer). The grid shown corresponds to a small portion of the image in Figure 3.3a.

C.2 Adding Constraints

In the constrained models the rate for each spin (timer) additionally depends on the state of its nearest neighbours. Only a minor adjustment to our procedure is necessary: whenever a timer goes off both it *and* its neighbours should be reset,[27] with rates appropriate to the model.

For example, if the system in Figure C.1a was to realise the FA model, the rates of the clocks at x_0 and x_2 should (assuming they do not have other active neighbours) be 0 until τ_1, at which point they would be reset to have rates $1-c$ and c respectively. The updated schematic is shown in Figure C.2a. As before, after the simulation has run its course the state of each spin at $t_0, t_1, \ldots$ may be used to produce an image (Figure C.2b).

D Operator Methods

D.1 Rayleigh–Ritz Theorem

The eigenvalues $\lambda_0 \geq \lambda_1 \geq \ldots \geq \lambda_n$ of an $n \times n$ hermitian matrix $\widehat{W}$ satisfy [92]

$$\lambda_n \leq \frac{\langle V|\widehat{W}|V\rangle}{\langle V|V\rangle} \leq \lambda_0 \quad \text{for all nonzero}^{28}\ |V\rangle\,, \tag{D.1}$$

$$\lambda_1 = \max_{|V\rangle \neq \mathbf{0}} \frac{\langle V|\widehat{W}|V\rangle}{\langle V|V\rangle} \tag{D.2}$$

and

$$\lambda_n = \min_{|V\rangle \neq \mathbf{0}} \frac{\langle V|\widehat{W}|V\rangle}{\langle V|V\rangle} \tag{D.3}$$

Here $|V\rangle = \sum_{\mathcal{C}} V(\mathcal{C})\,|C\rangle$ has coefficients $V(\mathcal{C}) \in \mathbb{C}^n$. Proof may be found in any standard textbook on linear algebra or matrix theory ([93, 94] are accessible).

D.2 Symmetrising $\widehat{W}$

Recalling the property of detailed balance (3.12)

$$P_{\text{eq}}(\mathcal{C})\,W(\mathcal{C} \to \mathcal{C}') = P_{\text{eq}}(\mathcal{C}')\,W(\mathcal{C}' \to \mathcal{C}) \tag{D.4}$$

and the definition of the matrix elements of $\widehat{W}$ (3.23)

$$W_{\mathcal{C}\mathcal{C}'} = \langle \mathcal{C}|\widehat{W}|\mathcal{C}'\rangle = e^{-s} W(\mathcal{C}' \to \mathcal{C}) - r(\mathcal{C})\,\delta_{\mathcal{C}\mathcal{C}'} \tag{D.5}$$

[27] In fact, beyond computational overhead there is nothing stopping us from resetting *all* of the timers, thanks to the memoryless property of the exponential distribution:

$$P\left(\tau = t + t' | \tau > t'\right) = P(\tau = t) \tag{C.4}$$

i.e. the probability that we need to wait another t seconds for a spin to flip, given that it has not done so after t' seconds, is equal to the probability of the spin flipping after t seconds on its own right.

[28] Note the condition $|V\rangle \neq \mathbf{0}$ (meaning at least one $V(\mathcal{C}) \neq 0$) is separate from that of $|V\rangle$ not containing the null configuration asserted in our application for irreducibility (meaning $V(\mathcal{C}) = 0$ for $\mathcal{C} : n_i = 0\ \forall i$).

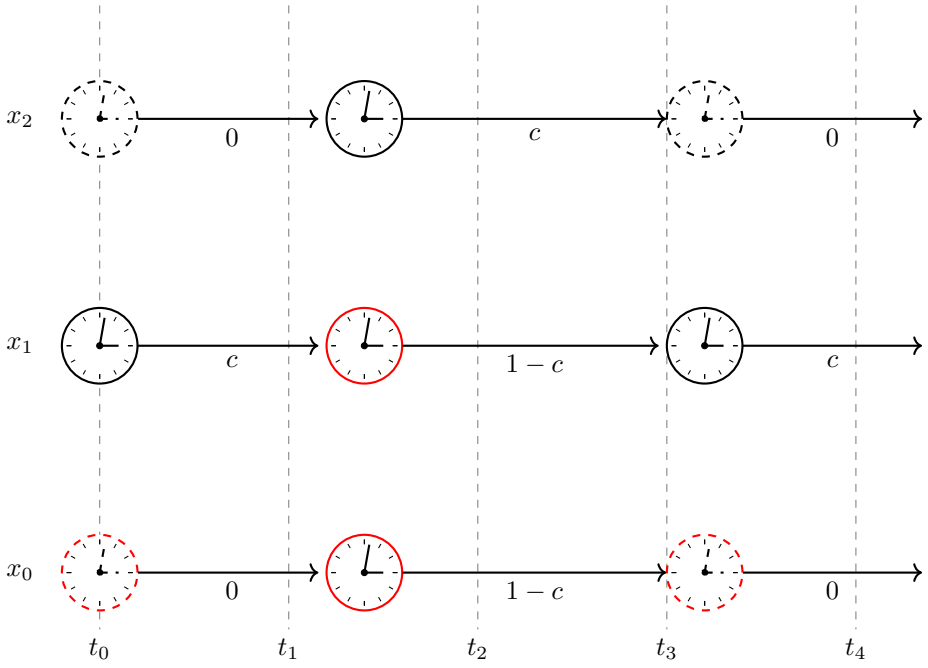

(a)

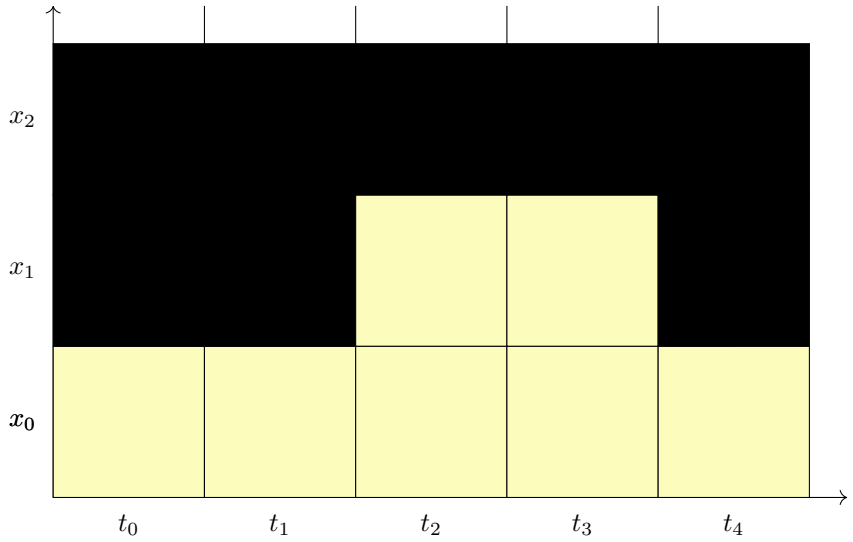

(b)

Figure C.2: Incorporating constraints (FA model in $d = 1$). (a) Assuming the spin at x_0 and x_2 have no other active neighbours, they are initially forbidden from changing state, indicated here as timers with broken lines. This is the case until the timer at x_1 (facilitated by that at x_0) sets off, at which point all three timers are reset with the rates shown. (b) The resulting image.

we have

$$\widetilde{W}_{\mathcal{C}\mathcal{C}'} = P_{\mathrm{eq}}(\mathcal{C})^{-1/2}\,\widehat{W}_{\mathcal{C}\mathcal{C}'}P_{\mathrm{eq}}(\mathcal{C}')^{1/2} \tag{D.6}$$

$$= e^{-s}P_{\mathrm{eq}}(\mathcal{C})^{-1/2}\,W(\mathcal{C}'\to\mathcal{C})^{1/2}\overbrace{W(\mathcal{C}'\to\mathcal{C})^{1/2}\,P_{\mathrm{eq}}(\mathcal{C}')^{1/2}}^{=P_{\mathrm{eq}}(\mathcal{C})^{1/2}W(\mathcal{C}\to\mathcal{C}')^{1/2}} - r(\mathcal{C})\,\delta_{\mathcal{C}\mathcal{C}'}\left[\frac{P_{\mathrm{eq}}(\mathcal{C}')}{P_{\mathrm{eq}}(\mathcal{C})}\right]^{1/2} \tag{D.7}$$

$$= e^{-s}\left[W(\mathcal{C}\to\mathcal{C}')\,W(\mathcal{C}'\to\mathcal{C})\right]^{1/2} - r(\mathcal{C})\,\delta_{\mathcal{C}\mathcal{C}'} \tag{D.8}$$

E Closed Quantum Systems

E.1 Entanglement Entropy

In quantum statistical mechanics, an ensemble of states is described by a density matrix operator

$$\rho(t) = \sum p_i\,|\psi_i\rangle\langle\psi_i| \tag{E.1}$$

where p_i $(1 \le i \le d)$ is the probability of the state $|\psi_i\rangle$ [95]. If all $p_i = 0$ except one then the state of the system is said to be *pure*. Otherwise, it is mixed.

The density matrix contains complete information of the statistics of a quantum system. A natural extension of entropy from classical probability theory is the *von Neumann entropy* [96]

$$S(t) = -\operatorname{Tr}[\rho\ln\rho] \tag{E.2}$$

This may be shown to vanish for a pure state and be maximised by a uniform distribution of states [97]. In this way S measures the extent to which the system fails to be in a pure state.

For pure states ($S = 0$) of a closed quantum system, such as those we encounter with the quantum East model, a second entropic quantity is defined as follows: divide the system into two parts A and B (Figure E.1) and perform a trace over the states of one subsystem (say B) to obtain a *reduced* density matrix for the other

$$\rho_A(t) = \operatorname{Tr}_B\rho \tag{E.3}$$

The von Neumann entropy associated with ρ_A,

$$S_A(t) = \rho_A\ln\rho_A, \tag{E.4}$$

provides a measure of the entanglement between A and B and is known as the *entanglement entropy* [16]. Provided the composite system is pure $S_A = S_B$ [97] and this definition is unambiguous.

The entanglement entropy is found to increase rapidly to a maximum determined by the size of the smaller subsystem[29] for a thermalising system, whilst increasing logarithmically (i.e. slowly) in the case of MBL [59].

An accessible account of the von Neumann entropy and its properties may be found in the textbook on quantum information by Nielsen [97, Ch. 11]. Garrahan's lecture [16, Sec. 3] provides a brief introduction to the entanglement entropy in relation to thermalisation; for a more detailed discussion of the topic refer to the reviews [56–58].

[29] In particular, for the equal partitions of the chain of N spins considered in in Section 4.2, the expected saturation value for the average entanglement entropy is $\bar{S} \sim (N/2)\ln 2 - 1/2$ [98] (cf. Figure 4.5a where $N = 14$).

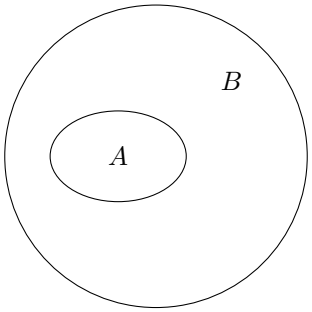

Figure E.1: Partition of a closed quantum system into two (generally unequal) parts. If the initial state of the total system is pure, it remains so for all times (unitary evolution) and the entanglement entropy $S_A(t)$ quantifies correlations between A and B.

E.2 Inverse Participation Ratio

Let $|\psi\rangle = \sum_k c_k |\varphi_k\rangle$ be the state of a quantum system expanded in an orthonormal basis $\{\varphi_k\}$. For the spin-chain considered in Section 4, $\{\varphi_k\}$ is simply the 2^N product kets describing all possible configurations of the spins. The extent of localisation of $|\psi\rangle$ with respect to this basis may be quantified by the inverse participation ratio (IPR) [99, 100]

$$\mathcal{I}(t) \propto \frac{1}{\sum_k |\langle\psi(t)|\varphi_k\rangle|^4} = \frac{1}{\sum_k |c_k|^4} \tag{E.5}$$

A large or small value of $\mathcal{I}$ indicates that the state is spread over many or few basis vectors, respectively. In general, for a state spread uniformly over ℓ basis vectors,

$$|\psi\rangle = \frac{1}{\sqrt{\ell}} \sum_{k=1}^{\ell} |\varphi_k\rangle \to \frac{1}{\sum_k |\langle\psi|\varphi_k\rangle|^4} = \frac{1}{\ell(1/\sqrt{\ell})^4} = \ell \tag{E.6}$$

Choices for the constant of proportionality in (E.5) vary; for the spin-chain $1/2^N$ was chosen so that $\mathcal{I}$ varies from unity for a completely delocalised state to $1/2^N$ in the case of perfect localisation:

$$|\psi\rangle = \frac{1}{2^{N/2}} \sum_k |\varphi_k\rangle \to \mathcal{I} = \frac{1}{2^N} \cdot 2^N = 1 \tag{E.7}$$

$$|\psi\rangle = |\varphi_j\rangle \to \mathcal{I} = \frac{1}{2^N} \cdot 1 = \frac{1}{2^N} \tag{E.8}$$

References

[1] H. Touchette, Phys. Rep. **478**, 1 (2009).

[2] R. L. Jack, Eur. Phys. J. B **93**, 74 (2020).

[3] G. Biroli and J. P. Garrahan, J. Chem. Phys. **138**, 12A301 (2013).

[4] R. Zallen, *The Physics of Amorphous Solids* (Wiley-VCH, 2004).

[5] J. P. Garrahan, R. L. Jack, V. Lecomte, E. Pitard, K. van Duijvendijk, and F. van Wijland, J. Phys. A Math. Theor. **42**, 075007 (2009).

[6] M. van Horssen, E. Levi, and J. P. Garrahan, Phys. Rev. B **92**, 100305 (2015).

[7] M. D. Donsker and S. R. S. Varadhan, Comm. Pure Appl. Math. **28**, 1 (1975).

[8] M. Freidlin and A. Wentzell, in *Random Perturbations of Dynamical Systems*, Vol. 260, Grundlehren der mathematischen Wissenschaften (Springer, New York, 1984).

[9] R. S. Ellis, *Entropy, Large Deviations, and Statistical Mechanics*, Vol. 271, Grundlehren der mathematischen Wissenschaften (Springer, New York, 1985).

[10] F. den Hollander, *Large deviations* (American Mathematical Society, Providence, R.I., 2000).

[11] J.-D. Deuschel and D. W. Stroock, *Large deviations* (Academic Press, Boston, Mass., 1989).

[12] R. S. Ellis, Scand. Actuar. J. **1995**, 97 (1995).

[13] P. Dupuis and R. S. Ellis, *A weak convergence approach to the theory of large deviations* (Wiley, New York, 1997).

[14] S. Whitelam, Phys. Rev. E **97**, 062109 (2018).

[15] D. Nickelsen and H. Touchette, Phys. Rev. Lett. **121**, 090602 (2018).

[16] J. P. Garrahan, Physica A **504**, 130 (2018).

[17] R. T. Rockafellar, *Convex Analysis* (Princeton University Press, Princeton, New Jersey, 1970).

[18] A. W. Roberts and D. Varberg, *Convex Functions* (Academic Press Inc, New York, Dec. 1973).

[19] H. Touchette, *Legendre-Fenchel transforms in a nutshell*, tech. rep. (University of London, London, 2005).

[20] E. R. Weeks, ACS Macro Lett. **6**, 27 (2017).

[21] C. Coulais, R. Candelier, and O. Dauchot, AIP Conf. Proc. **1542**, 25 (2013).

[22] T. E. Angelini, E. Hannezo, X. Trepat, M. Marquez, J. J. Fredberg, and D. A. Weitz, Proc. Natl. Acad. Sci. U.S.A. **108**, 4714 (2011).

[23] G. Biroli and J. P. Bouchaud, arXiv:0912.2542 (2009).

[24] D. Chandler and J. P. Garrahan, Annu. Rev. Phys. Chem. **61**, 191 (2010).

[25] J. Shelby, *Introduction to Glass Science and Technology*, 2nd ed. (The Royal Society of Chemistry, 2005), pp. 11–21.

[26] Y. S. Elmatad, D. Chandler, and J. P. Garrahan, J. Phys. Chem. B **114**, 17113 (2010).

[27] D. J. Plazek, C. A. Bero, and I.-C. Chay, J. Non Cryst. Solids **172-174**, 181 (1994).

[28] K. Ngai, *Relaxation and Diffusion in Complex Systems*, Vol. 15, Partially Ordered Systems 1212 (Springer, 2011).

[29] C. A. Angell, K. L. Ngai, G. B. McKenna, P. F. McMillan, and S. W. Martin, J. Appl. Phys. **88**, 3113 (2000).

[30] K. A. Connors, *Chemical Kinetics The Study of Reaction Rates in Solution* (VCH, 1990).

[31] K. Binder and W. Kob, *Glassy Materials and Disordered Solids An Introduction to Their Statistical Mechanics* (World Scientific, 2005).

[32] A. S. Keys, L. O. Hedges, J. P. Garrahan, S. C. Glotzer, and D. Chandler, Phys. Rev. X **1**, 021013 (2011).

[33] S. Karmakar, C. Dasgupta, and S. Sastry, Rep. Prog. Phys. **79**, 016601 (2016).

[34] J. P. Garrahan, R. L. Jack, V. Lecomte, E. Pitard, K. van Duijvendijk, and F. van Wijland, Phys. Rev. Lett. **98**, 195702 (2007).

[35] G. H. Fredrickson and H. C. Andersen, Phys. Rev. Lett. **53**, 1244 (1984).

[36] J. P. Garrahan, P. Sollich, and C. Toninelli, in *Dynamic heterogeneities in glasses, colloids and granular media*, edited by L. Berthier, G. Biroli, J.-P. Bouchaud, L. Cipelletti, and W. V. Saarloos, International Series of Monographs on Phyiscs 150 (Oxford Science Publications, 2011), pp. 68–109.

[37] P. Chleboun, A. Faggionato, and F. Martinelli, J. Stat. Mech. **2013**, L04001 (2013).

[38] F. Ritort and P. Sollich, Adv. Phys. **52**, 219 (2003).

[39] W. Kob and H. C. Andersen, Phys. Rev. E **48**, 4364 (1993).

[40] J. Jackle and A. Kronig, J. Phys. Condens. Matter **6**, 7633 (1994).

[41] C. Gardiner, *Stochastic Methods: A Handbook for the Natural and Social Sciences*, 4th ed., Springer Series in Synergetics (Springer, 2009).

[42] M. Merolle, J. P. Garrahan, and D. Chandler, Proc. Natl. Acad. Sci. U.S.A. **102**, 10837 (2005).

[43] L. O. Hedges, R. L. Jack, J. P. Garrahan, and D. Chandler, Science **323**, 1309 (2009).

[44] T. Nemoto, R. L. Jack, and V. Lecomte, Phys. Rev. Lett. **118**, 115702 (2017).

[45] R. L. Jack, T. Nemoto, and V. Lecomte, arXiv:1912.02465 (2019).

[46] R. L. Jack, J. P. Garrahan, and D. Chandler, J. Chem. Phys. **125**, 184509 (2006).

[47] V. Privman and M. E. Fisher, J. Stat. Phys. **33**, 385 (1983).

[48] C. Borgs and R. Kotecký, J. Stat. Phys. **61**, 79 (1990).

[49] W. Kob and H. C. Andersen, Phys. Rev. Lett. **73**, 1376 (1994).

[50] U. R. Pedersen, T. B. Schrøder, and J. C. Dyre, Phys. Rev. Lett. **120**, 165501 (2018).

[51] R. L. Jack, L. O. Hedges, J. P. Garrahan, and D. Chandler, Phys. Rev. Lett. **107**, 275702 (2011).

[52] T. Speck and D. Chandler, J. Chem. Phys. **136**, 184509 (2012).

[53] T. Speck, A. Malins, and C. P. Royall, Phys. Rev. Lett. **109**, 195703 (2012).

[54] F. Turci, C. P. Royall, and T. Speck, Phys. Rev. X **7**, 031028 (2017).

[55] Y. S. Elmatad, R. L. Jack, D. Chandler, and J. P. Garrahan, Proc. Natl. Acad. Sci. U.S.A. **107**, 12793 (2010).

[56] D. A. Abanin, E. Altman, I. Bloch, and M. Serbyn, Rev. Mod. Phys. **91**, 021001 (2019).

[57] C. Gogolin and J. Eisert, Rep. Prog. Phys. **79**, 056001 (2016).

[58] L. D'Alessio, Y. Kafri, A. Polkovnikov, and M. Rigol, Adv. Phys. **65**, 239 (2016).

[59] R. Nandkishore and D. A. Huse, Annu. Rev. Condens. Matter Phys. **6**, 15 (2015).

[60] F. Alet and N. Laflorencie, C. R. Phys. **19**, 498 (2018).

[61] D. J. Luitz and Y. B. Lev, Ann. Phys. **529**, 1600350 (2017).

[62] A. Pal and D. A. Huse, Phys. Rev. B **82**, 174411 (2010).

[63] C. L. Henley, J. Phys. Condens. Matter **16**, S891 (2004).

[64] C. Castelnovo, C. Chamon, C. Mudry, and P. Pujol, Ann. Phys. **318**, 316 (2005).

[65] D. S. Rokhsar and S. A. Kivelson, Phys. Rev. Lett. **61**, 2376 (1988).

[66] J. M. Hickey, S. Genway, and J. P. Garrahan, J. Stat. Mech. **2016**, 054047 (2016).

[67] J. R. Garrison, R. V. Mishmash, and M. P. A. Fisher, Phys. Rev. B **95**, 054204 (2017).

[68] R. Mondaini and Z. Cai, Phys. Rev. B **96**, 035153 (2017).

[69] C. P. Royall, F. Turci, S. Tatsumi, J. Russo, and J. Robinson, J. Phys. Condens. Matter **30**, 363001 (2018).

[70] D. Coslovich and R. L. Jack, J. Stat. Mech. **2016**, 074012 (2016).

[71] A. S. Keys, A. R. Abate, S. C. Glotzer, and D. J. Durian, Nat. Phys. **3**, 260 (2007).

[72] A. J. Liu and S. R. Nagel, Annu. Rev. Condens. Matter Phys. **1**, 347 (2010).

[73] R. Das, I. Tah, and S. Karmakar, J. Chem. Phys. **149**, 024501 (2018).

[74] H. B. Yu, W. H. Wang, H. Y. Bai, and K. Samwer, Natl Sci. Rev. **1**, 429 (2014).

[75] C. K. Mishra, X. Ma, P. Habdas, K. B. Aptowicz, and A. G. Yodh, Phys. Rev. E **100**, 020603 (2019).

[76] R. Gutierrez, J. P. Garrahan, and R. L. Jack, J. Stat. Mech. **2019**, 094006 (2019).

[77] J. P. Garrahan and I. Lesanovsky, Phys. Rev. Lett. **104**, 160601 (2010).

[78] A. J. Daley, Adv. Phys. **63**, 77 (2014).

[79] Z. K. Minev, S. O. Mundhada, S. Shankar, P. Reinhold, R. Gutiérrez-Jáuregui, R. J. Schoelkopf, M. Mirrahimi, H. J. Carmichael, and M. H. Devoret, Nature **570**, 200 (2019).

[80] F. Carollo, R. L. Jack, and J. P. Garrahan, Phys. Rev. Lett. **122**, 130605 (2019).

[81] A. A. Zvyagin, J. Low Temp. Phys. **42**, 971 (2016).

[82] I. Lesanovsky and J. P. Garrahan, Phys. Rev. Lett. **111**, 215305 (2013).

[83] C. Pérez-Espigares, I. Lesanovsky, J. P. Garrahan, and R. Gutiérrez, Phys. Rev. A **98**, 021804 (2018).

[84] W. Rudin, *Real & Complex Analysis*, English, 3rd ed. (Mcgraw Hill Higher Education, New Delhi etc., 1987).

[85] M. Capinski and P. E. Kopp, *Measure, Integral and Probability*, 2nd ed., Springer Undergraduate Mathematics Series (Springer-Verlag, London, 2004).

[86] S. M. Rekhson, in *Viscosity and Relaxation*, Vol. 3, edited by D. R. Uhlmann and N. J. Kreidl, Glass: Science and Technology (Academic Press Inc, Orlando, Florida, 1986), pp. 1–117.

[87] D. H. Uhlmann and N. J. Kreidl, eds., *Viscoelasticity and Relaxation*, Vol. 3, Glass: Science and Technology (Academic Press Inc., Orlando, Florida, 1986).

[88] E. L. Bourhis, *Glass: Mechanics and Technology*, 2nd ed. (Wiley VCH, Weinheim, Sept. 2014).

[89] L. Berthier, G. Biroli, J.-P. Bouchaud, and R. L. Jack, in *Dynamic Heterogeneities in Glasses, Colloids and Granular Media*, edited by L. Berthier, G. Biroli, J.-P. Bouchaud, L. Cipelletti, and W. V. Saarloos, International Series of Monographs on Phyiscs 150 (Oxford Science Publications, 2011), pp. 68–109.

[90] S. Karmakar, C. Dasgupta, and S. Sastry, Annu. Rev. Condens. Matter Phys. **5**, 255 (2014).

[91] G. Grimmett and D. Stirzaker, *Probability and random processes*, 3rd ed. (Oxford University Press, USA, 2001), 608 pp.

[92] "Hermitian and positive definite matrices", in *Handbook of linear algebra*, edited by L. Hogben and K. H. Rosen, 2nd ed., Discrete Mathematics And Its Applications (CRC Press, 2014) Chap. 9, pp. 164–177.

[93] C. D. Meyer, *Matrix analysis and applied linear algebra* (Society for Industrial and Applied Mathematics, 2000).

[94] C. R. Johnson and R. A. Horn, *Matrix analysis*, 2nd ed. (Cambridge University Press, Cambridge, United Kingdom, 2013).

[95] R. Shankar, *The principles of quantum mechanics*, 2nd ed. (Springer, 1994).

[96] J. v. Neumann, Nachr. Akad. Wiss. Gott. Philol. Hist. Kl., 273 (1927).

[97] M. A. Nielsen and I. L. Chuang, *Quantum computation and quantum information*, 1st ed., Cambridge Series on Information and the Natural Sciences (Cambridge University Press, 2004).

[98] D. N. Page, Phys. Rev. Lett. **71**, 1291 (1993).

[99] F. Wegner, Z. Phys. B **36**, 209 (1980).

[100] F. Dukesz, M. Zilbergerts, and L. F. Santos, New J. Phys. **11**, 043026 (2009).